Modelling and measurements relevant for transport of polarized light in skin tissue

Anak Bahadur Bhandari

Dissertation submitted for the degree of Philosophiae Doctor (PhD)

Department of Physics and Technology

University of Bergen

November - 2011

Contents

List of Figures

Acknowledgements

There are many people who have given their time, talents, and support to assist me in an unselfish manner throughout my study. First and foremost I wish to thank Professor Emeritus Yngvar Gjessing, Department of Geophysics, University of Bergen for his inspiration and encouragement. This dissertation would not have become a reality unless Professor Yngvar had asked me to meet Professor Jakob Stamnes in the Department of Physics and Technology. It was his inspiration that made this study a thought to reality.

My sincere gratitude and appreciation to my supervisor, Professor Jakob Stamnes, and co-supervisor, Associate Professor Øyvind Frette, for their continuous teaching and guidance throughout the study period. I would like to extend my gratitude also to Professor Knut Stamnes, Steven Institute of Technology, USA for his ideas and knowledge, which are central to this thesis. I am thankful to Associate Professor Jan Asle Olseth in the Department of Geophysics for his guidance in preparing a seminar on meteorological instruments.

Dozens of people have helped and taught me through these years. I would like to thank all who have assisted me in some way or another. I am grateful to the entire optics group. Being part of that group has helped me learn a lot. Thank you for sharing your wisdom and expertise with me. I am sincerely thankful to the people working in the administration. My special thanks to Terje Finnekås for his counseling and Villy Nielsen for his evergreen positive humor.

Last but certainly not least, I heartily thank my wife Chandana and my daughter Anja for their patience and continuous support. Their support has been unconditional all these years; and they have given up many things for me; they have cherished with me every great moment and supported me whenever I needed it. The most inspirational word which kept me going were from my four years old daughter - 'min pappa pleier å gå på jobb to ganger om dagen og alltid i helgen."

Anak Bhandari
Bergen, November 2011

List of papers

1. Anak Bhandari, Børge Hamre, Øyvind Frette, Lu Zhao, Jakob J. Stamnes, and Morten Kildemo. *Bidirectional reflectance distribution function of Spectralon white reflectance standard illuminated by incoherent unpolarized and plane-polarized light.* Applied Optics **50**, 2431-2442 (2011).

2. Anak Bhandari, Børge Hamre, Øyvind Frette, Knut Stamnes, and Jakob J. Stamnes. *Modeling optical properties of human skin using Mie theory for particles with different size distributions and refractive indices.* Optic Express **19**, 14549-14567 (2011).

3. Anak Bhandari, Snorre Stamnes, Øyvind Frette, Knut Stamnes, and Jakob J. Stamnes. *The Stokes scattering matrix for human skin computed from Mie scattering method.* To be submitted for publication.

4. Kristian P. Nielsen, Lu Zhao, Anak Bhandari, Børge Hamre, and Jakob J. Stamnes and Knut Stamnes *Spectral radiance imaging of human skin tissue: theoretical sspects and empirical results.* Presented at "Optical Imaging 2006 - Fifth Inter-Institute Workshop on Optical Diagnostic Imaging from Bench to Beside at the National Institutes of Health". Organized by SPIE (2006). Abstract at p. 101 of workshop program.

Chapter 1

Introduction

The group of optics and atomic physics at the Department of Physics and Technology, University of Bergen has been actively involved in research and development of non-invasive biomedical techniques to identify early stage malignant melanomas from non-malignant or benign skin lesions. Such optical diagnostic technique [1, 2] relies on scalar radiative transfer theory, which has been developed and extensively used in the field of atmospheric remote sensing based optical satellite measurements. In order to use similar radiative transfer techniques in an optical probing thechnique to investigate skin tissue disorders, one must take into account the interaction of electromagnetic radiation with skin tissue. Having the correct knowledge of absorption and scattering properties of heterogeneous skin tissue, one may optically probe a coupled air-skin system in a similar manner as in satellite remote sensing of a coupled atmosphere-ocean system. The only important difference between these two systems is that the skin is a moderately denser optical medium than the ocean, implying that existing radiative transfer models for coupled atmosphere-ocean remote sensing can be applied to an air-skin system with some adjustments [3, 4].

Investigations of atmospheric remote sensing have indicated that the use of scalar radiative transfer models poses uncertainties in the calculation of the planetary scattering phase function, which increase with the scattering angle [5] defined as the angle between the incident starlight and the observer. The polarization effects in scattered light can provide useful information about scattering media. Thus, the use of polarized light instead of natural or unpolarized light in optical sensing of a coupled air-skin system can improve the characterization of size and shape distributions of scattering particles in the skin.
The goal of this thesis is intended to investigate skin optics relevant for the transport of polarized light into the layered structure of human skin.

1.1 Light

Light illuminates objects around us, and the scattered light from objects make them visible. Light is electromagnetic radiation in the wavelength range of $\lambda = 400 - 700$ nm [see Fig 1.1]. Only this small range of the electromagnetic radiation spectrum is visually sensitive to human eyes in different colors, whereas the spectral distribution of entire electromagnetic radiation ranges from very short gamma rays ($\lambda \leq 10^{-12}$ nm) to long radio waves ($\lambda \geq 10^{4}$ m). The most important parts of the electromagnetic radiation in our earth-atmosphere system belongs to the ultraviolet (UV), visible (VIS), and near-infrared (NIR) spectral regions. The UV part of the electromagnetic radiation is further divided into UVA radiation in the wavelength range from $\lambda = 400$ to 320 nm, UVB radiation in the wavelength range from $\lambda = 320$ to 280 nm, and UVC radiation in the wavelength range from $\lambda = 200$ to 280 nm. All parts of the electromagnetic radiation travel at a constant speed $c = 3 \times 10^{8}$ m/s in free space, and takes about 8.3 minutes to reach the earth from the sun (the earth-sun distance is 1 AU $\simeq 15 \times 10^{7}$ km. The propagation through any material medium is affected by the refractive index n of the material in accordance with the relation $v = c/n$, where v is the speed of light in a material medium. The value of n is 1.000 in vacuum and is greater than 1.000 in a material. However, the frequency ν does not change, so that light of different frequencies ν travels at different speeds v in the same material medium.

Light can show both wave-like and particle-like character. The wave-particle duality, is manifested in the following relation

$$\lambda = \frac{h}{p} \tag{1.1}$$

where $h = 6.622607 \times 10^{-34}$ J s is Planck's constant, and $p = E/c$ is the momentum of a photon with speed c and energy E. The wavelength λ in Eq. (1.1) associated with a moving photon is called the *de-Broglie* wavelength [6], and the energy E carried by each photon is quantized to discrete values of $h\nu$, where ν is the frequency of the radiation. Since $\lambda\nu = c$, photos with high energy have short wavelength, and vice-versa.

The particle-wave duality is often attributed to a high energy photon. In this thesis, the light is treated as electromagnetic wave whose spectral distribution is shown in Fig. 1.1.

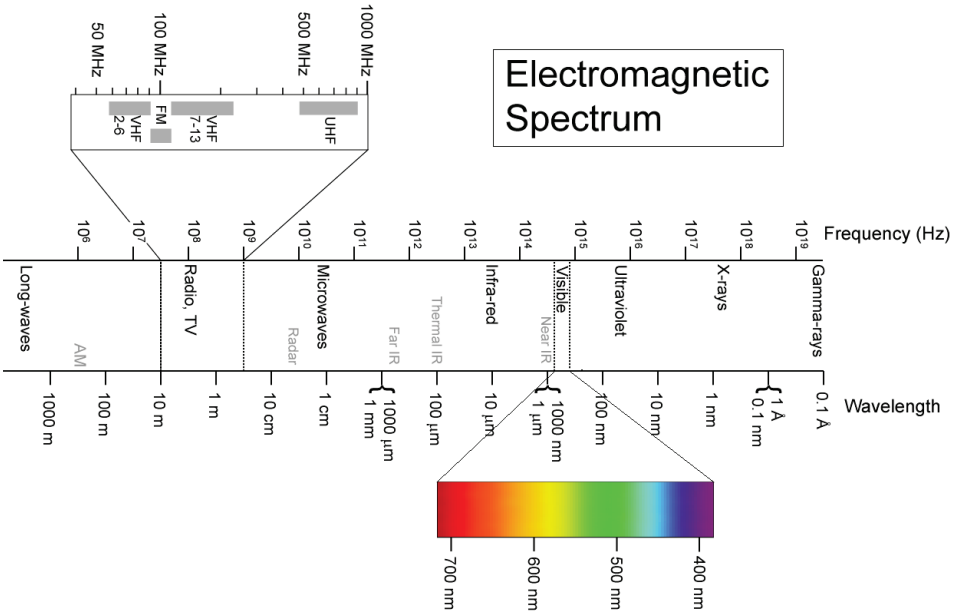

Figure 1.1: Spectral distribution of electromagnetic radiation divided into different wavelengths and frequency bands. Adapted from Wikipedia [7].

1.2 Electromagnetic properties of light

Light consists of transverse electromagnetic waves, each comprised of an electric field vector $\vec{E}$ and a magnetic induction or magnetic flux density vector $\vec{B}$, which oscillate mutually perpendicular to each other and to the direction of propagation. The direction of propagation is given by their cross product $\vec{S} = \vec{E} \times \vec{B}$, where $\vec{S}$ is called the Poynting vector after the name of J. H. Poynting (1852 - 1914). The $\vec{S}$ gives the instantaneous value of the light energy flowing through a unit area that is perpendicular to the propagation direction. The instantaneous energy carried by the electric and magnetic field vectors is oscillating very rapidly with time. For example, red light with $\lambda = 700$ nm oscillates 4.28×10^{14} cycles in one second. Therefore, the light energy or *irradiance* I is usually measured as the time averaged magnitude of the poynting vector, i.e.

$$I =< S >= \frac{c\,\epsilon_0}{2} E^2 \qquad [\mathrm{Wm}^{-2}] \tag{1.2}$$

where $\epsilon_0 = 8.85 \times 10^{-12}$ Fm^{-1} is the free space permitivity. The magnitudes of $\vec{E}$ and $\vec{B}$ in free space are connected by $E = cB$. Thus, the Poynting vector gives the direction of the electromagnetic energy flow, and the time-averaged magnitude of the Poynting vector is the intensity or radiance.

The behavior of the electromagnetic field vectors $\vec{E}$ and $\vec{B}$ in a material medium is described by Maxwell's equations [8], and the additional material equations or constitutive relations

$$\vec{j} = \sigma \vec{E} \tag{1.3a}$$

$$\vec{D} = \epsilon \vec{E} \tag{1.3b}$$

$$\vec{B} = \mu \vec{H} \tag{1.3c}$$

where j is the electric current density, σ the electric conductivity, D the electrical displacement, ϵ the electric permittivity, μ the magnetic permeability, and H the magnetic field.

The optical properties of a material medium depends on the quantities ϵ and μ through the refractive index n, given by $n = \sqrt{\epsilon\mu}$. For frequencies in the visible range, most dielectric materials have $\mu \simeq 1$, so the optical properties are related only to the dielectric permittivity. In a homogeneous and isotropic dielectric medium, ϵ is a scalar constant at a given frequency, implying that it does not vary with the position or with the direction of light propagation, so that the speed of light is independent of its direction. On the other hand, ϵ varies with the propagation direction of light in an anisotropic medium, so that the relation between $\vec{D}$ and $\vec{E}$ in Eq. (1.3b) does not hold. In such a medium, the permittivity becomes a tensor, implying that $\vec{D}$ in general is not parallel to $\vec{E}$ [9, 10].

A substance with a negligible value of the conductivity σ is called a dielectric.

1.3 Polarization properties of light

Natural light consists of a number of plane polarized waves, each oscillating rapidly in such a way that its polarization is completely unpredictable. As mentioned previously, red light of $\lambda = 700$ nm will oscillate 4.28×10^{14} cycles per second. The response time of a light detector to measure each cycle would have to be extremely short. Thus, a detector with an integration time of the order of a *milli*second will average over many monochromatic oscillations.

To account for the polarization, we need to consider the amplitude and the phase of propagating light wave. The plane of polarization is determined by the direction of oscillation of $\vec{E}$ and the direction of propagation. The end point of $\vec{E}$ rotates rapidly and changes its magnitude in such a way that the locus of the points whose coordinates are $E_x = a_x \cos(\alpha+\delta_1)$ and $E_y = a_y \cos(\alpha+\delta_2)$ trace out a conic section of the form [8,9]

$$\left(\frac{E_x}{a_x}\right)^2 + \left(\frac{E_y}{a_y}\right)^2 - 2\cos\delta \left(\frac{E_x}{a_x}\right)\left(\frac{E_y}{a_y}\right) = \sin^2\delta \tag{1.4}$$

where $a_x > 0$ and $a_y > 0$ are instantaneous E-field amplitudes along the $\hat{x}$ and $\hat{y}$ directions, respectively, in a right-handed co-ordinate system where the direction of propagation is along $\hat{z} = \hat{x} \times \hat{y}$ direction, which points out of the page in Fig. 1.2.

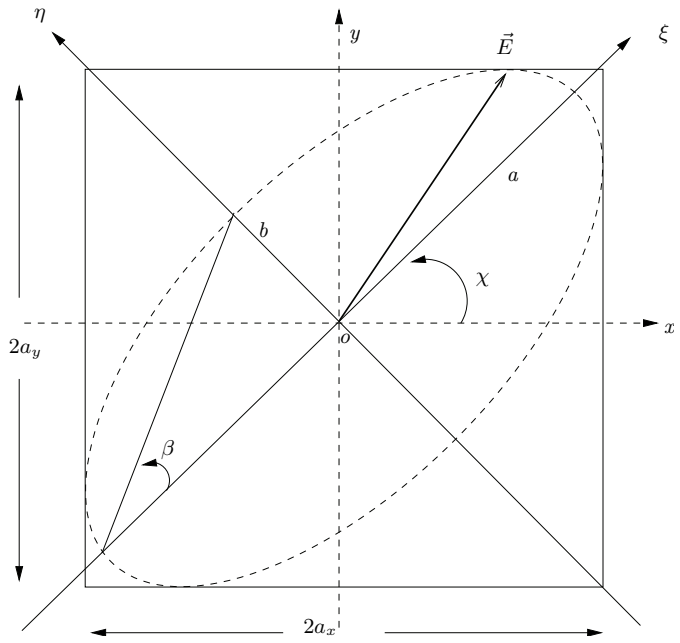

Figure 1.2: Elliptically polarized light. The end point of the electric field vector $\vec{E}$ traces out a vibration ellipse as it oscillates. The angle χ $(0 \le \chi \le \pi)$ gives the inclination of the ellipse with respect to the x axis of the right-handed cartesian co-ordinate system.

The phase difference is given by $\delta = \delta_2 - \delta_1$ and $\alpha = \omega t - kz$ is variable phase factor. The angle χ of inclination of the ellipse with the x axis is given by

$$\tan 2\chi = \frac{2a\,b}{a^2 - b^2}\cos\delta. \tag{1.5}$$

When $\delta = \pi/2$ and $a_x = a_y$, Eq. (1.4) reduces to the equation of a circle. For $\delta = 0$ or π, Eq. (1.4) degenerates into straight lines of the form $E_y = \pm(a_y/a_x)E_x$, where $\pm(a_y/a_x)$ is the slope. When the slope is positive (negative), light is linearly polarized in the horizontal (vertical) plane.

The ratio of semi-major axis a and semi-minor axis b of the ellipse [see Fig 1.2], *i.e.*, $\tan\beta = b/a$ where $-\pi/4 \leq \beta \leq \pi/4$, determines the shape of the ellipse. When $\beta = \pi/4$, the light becomes circularly polarized, and the circular polarization is right handed if $\beta = \pi/4$ and left handed if $\beta = -\pi/4$. The sum of right-handed and left-handed circular polarized light gives linearly polarized light. Thus, the general polarization state of light, occurring when the x and y components of electric field amplitudes are not equal and also when the phase difference $\delta \neq \pm\pi/2$, is elliptical polarization. If we know the length of the semi-axes (a, b) and the orientation (χ) of the polarization ellipse, the phase difference can be determined [8] from Eq. (1.5).

1.3.1 Stokes vector representation of polarized light

The polarization states of a *quasi-monochromatic* light wave can be represented by a 4×1 vector, called the Stokes vector $\mathbf{S}$, whose elements I, Q, U, and V are called the Stokes parameters [8,11], originally after G. G. Stokes in 1852. The Stokes parameters are independent of each other, separately measurable as intensities, and related to the transverse components of complex electric field $\vec{E}$=$(E_\perp + E_\parallel)\mathrm{e}^{i(kz-\omega t)}$ in the following form [10]

$$\begin{bmatrix} I \\ Q \\ U \\ V \end{bmatrix} = \begin{bmatrix} \langle E_\parallel E_\parallel^* \rangle + \langle E_\perp E_\perp^* \rangle \\ \langle E_\parallel E_\parallel^* \rangle - \langle E_\perp E_\perp^* \rangle \\ \langle E_\parallel E_\perp^* \rangle + \langle E_\perp E_\parallel^* \rangle \\ i(\langle E_\parallel E_\perp^* \rangle - \langle E_\perp E_\parallel^* \rangle) \end{bmatrix}. \tag{1.6}$$

Here the electric field components $E_\perp$ and $E_\parallel$ are perpendicular and parallel to the plane of scattering, *i.e.* the plane defined by the directions of the incident light and the scattered light. The symbol *asterisk* denotes the complex conjugate, the notation $\langle\ \rangle$ indicates the time average, and $i = \sqrt{-1}$ is the imaginary unit.

The first parameter $I \geq 0$ is the total intensity, the parameters Q and the U describe the directions of linear polarization, and the parameter V describes the circular polarization [12]. The Stokes parameters are real physical quantities of the same dimension.

However, they can be normalized to I in order to make their values dimensionless in the range between 1 and -1. Stokes vectors for different polarization states in the normalized representation are given in Table 1.1.

Table 1.1: Normalized Stokes vectors for different polarization states.

Stokes parameters	Horizontal linear	Vertical linear	+45° linear	-45° linear	Right circular	Left circular
$\begin{bmatrix} I \\ Q \\ U \\ V \end{bmatrix}$	$\begin{bmatrix} 1 \\ 1 \\ 0 \\ 0 \end{bmatrix}$	$\begin{bmatrix} 1 \\ -1 \\ 0 \\ 0 \end{bmatrix}$	$\begin{bmatrix} 1 \\ 0 \\ 1 \\ 0 \end{bmatrix}$	$\begin{bmatrix} 1 \\ 0 \\ -1 \\ 0 \end{bmatrix}$	$\begin{bmatrix} 1 \\ 0 \\ 0 \\ 1 \end{bmatrix}$	$\begin{bmatrix} 1 \\ 0 \\ 0 \\ -1 \end{bmatrix}$

The Stokes parameters satisfy the criterion $I^2 \geq Q^2 + U^2 + V^2$ for any arbitrary polarization state of light. For completely polarized light, $I^2 = Q^2 + U^2 + V^2$ and for completely unpolarized light, $Q = U = V = 0$. Therefore, the degree to which the light is polarized is given by the degree of polarization P which is defined as the ratio of average intensity of completely polarized light to the averaged total intensity.
If the incident light is unpolarized, the degree of polarization P of the scattered light is measured as

$$P = \frac{I_\perp - I_\parallel}{I_\perp + I_\parallel} \tag{1.7}$$

where $I_\perp = \langle E_\perp E_\perp^* \rangle$ and $I_\parallel = \langle E_\parallel E_\parallel^* \rangle$ are the perpendicular and parallel components of the scattered intensity with respect to the plane of scattering. The intensity I of natural light is equivalent to the sum of its orthogonal components $I_\parallel$ and $I_\perp$, *i.e.* $I = I_\parallel + I_\perp$. Generally, the polarization for which the $\vec{E}$ field is normal to the plane of incidence is called s polarization (from German "Senkrecht") or TE ("transverse electric") polarization and that for which the $\vec{E}$ field is parallel to the plane of incidenc is called p polarization or TM ("transverse magnetic") polarization.

The value of the degree of polarization P lies in the range of $-1 \leq P \leq 1$. If $P = 0$, the light is unpolarized or depolarized and if $|P| < 1$, it is partially polarized. If $P > 0\,(P < 0)$, the light is polarized perpendicular (parallel) to the scattering plane, and $|P| = 1$ corresponds to complete polarization.

The Stokes vector in Eq. (1.6) is given by $\mathbf{S} = \{I\ Q\ U\ V\}^T$, where $I = I_\parallel + I_\perp$ and

$Q = I_{\parallel} - I_{\perp}$. The degree of polarization in terms of the Stokes parameters is given by

$$P = \left\{ \begin{array}{ll} \frac{(Q^2+U^2+V^2)^{\frac{1}{2}}}{I} & \text{for elliptical polarization} \\ \\ \frac{(Q^2+U^2)^{\frac{1}{2}}}{I} & \text{for linear polarization} \\ \\ \frac{V}{I} & \text{for circular polarization} \end{array} \right\}. \tag{1.8}$$

A monochromatic plane wave is completely polarized. An arbitrary state of polarized light is the sum of a partially polarized part and completely polarized part. Polarization states of light in terms of normalized Stokes parameters can be geometrically represented on the surface of the Poincare sphere [9].

1.4 Interaction of light with matter

We observe objects around us by means of how light interacts with various materials through absorption, reflection, and scattering. The interaction of light or an electromagnetic wave with matter is described in terms of absorption, reflection, refraction, scattering, and dispersion. When light travels from one medium to another medium of different refractive index, the light will be reflected and refracted at the interface depending on the boundary conditions such that

(1) the normal component of $\vec{B}$ and tangential component of $\vec{E}$ are continuous across the interface,

(2) the tangential component of $\vec{H}$ and the normal component of $\vec{D}$ may be discontinuous cross the interface. The electric displacement vector $\vec{D}$ will change as the result of a possible surface charge, and the magnetic field vector $\vec{H}$ will change as the result of a possible surface current density [9].

Within the medium, the light can be extinguished due to absorption and scattering. Moreover, the wavelength of the light changes when it propagates from one medium to another medium of different refractive index, however the frequency remains unchanged. The amplitude of a reflected or transmitted TE or TM plane waves is given in terms of the amplitude of the correspondingly polarized incident plane wave by Fresnel's equations [10].

1.4.1 Reflection and refraction

When light falls on a surface, part of it is reflected and part is refracted, as shown in the Fig 1.3(a). The reflection of light from a mirror-like surface is called specular

reflection for which the angle of reflection θ_r is equal to the angle of incidence θ_i. In the case of specular reflection, the incident, reflected, and transmitted directions lie in the same plane, which is called the plane of incidence and is defined by the directions of the incident light and the normal to the reflecting surface.

The light entering from the first medium into the second medium will continue in a direction different from its initial direction [Fig. 1.3(a)]. The relation between the angle

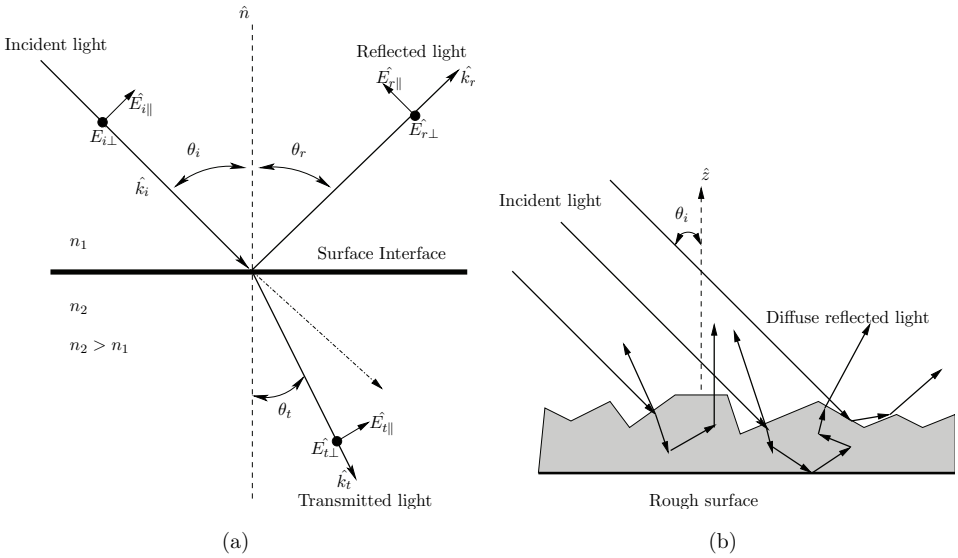

Figure 1.3: Reflection and refraction phenomena where (a) shows the reflection and refraction of light incident upon a plane surface interface and (b) shows multiple reflections from random micro-facets on a rough surface, for which $\hat{z}$ is the mean normal to the surface. In both cases θ_i is the angle of incidence.

of incidence θ_i and the angle of transmision θ_t is given by Snell's law

$$n_1 \sin\theta_i = n_2 \sin\theta_t. \tag{1.9}$$

If $n_1 > n_2$, the light transmitted from the interface will propagate in a direction defined by θ_t such that $\theta_t > \theta_i$, and if the angle of incidence becomes larger than $\theta_{ic} = \arcsin(n_2/n_1)$, the light will be totally reflected back to the same medium.

On the other hand, if $n_2 > n_1$, then $\theta_t < \theta_i$, and total reflection will not occur. The ratio between the amplitude of a reflected or refracted plane wave and that of the

incident plane wave is given by

$$r_{\parallel} = \frac{E_{\parallel r}}{E_{\parallel i}} = \frac{n_1 \cos\theta_t - n_2 \cos\theta_i}{n_1 \cos\theta_t + n_2 \cos\theta_i} \tag{1.10}$$

or

$$t_{\parallel} = \frac{E_{\parallel t}}{E_{\parallel i}} = \frac{2n_1 \cos\theta_i}{n_1 \cos\theta_t + n_2 \cos\theta_i} \tag{1.11}$$

when the $\vec{E}$ field is parallel to the plane of incidence. Similarly, when the $\vec{E}$ field is perpendicular to the plane of incidence, these ratios are

$$r_{\perp} = \frac{E_{\perp r}}{E_{\perp i}} = \frac{n_1 \cos\theta_i - n_2 \cos\theta_t}{n_1 \cos\theta_i + n_2 \cos\theta_t} \tag{1.12}$$

and

$$t_{\perp} = \frac{E_{\perp t}}{E_{\perp i}} = \frac{2n_1 \cos\theta_i}{n_1 \cos\theta_i + n_2 \cos\theta_t}. \tag{1.13}$$

The basic radiance (I/n^2) of light in a medium of refractive index n is invariant [14] provided that there is no reflecting interface along the light path. The basic radiance of the reflected light (I_r/n_1^2) in the medium of refractive index n_1 or of the transmitted light (I_t/n_2^2) in the medium of refractive index n_2 can be obtained by multiplying the basic radiance of the incident light (I_i/n_1^2) with the reflectance R or the transmittance T given by

$$R = \frac{r_{\parallel}^2 + r_{\perp}^2}{2} \quad ; \quad T = \frac{n_2 \cos\theta_t}{n_1 \cos\theta_i} \frac{t_{\parallel}^2 + t_{\perp}^2}{2}. \tag{1.14}$$

If there is no absorption, then $R + T = 1$.

When $n_2 > n_1$, the reflected light of incident polarization parallel to the plane of incidence vanishes at the particular value of $\theta_i = \theta_B$ for which $\theta_B + \theta_{tB} = \pi/2$ [see Fig 1.4]. This particular angle of incidence θ_B is referred to as the polarization angle or Brewster angle. Unpolarized light incident upon an interface $(n_2 > n_1)$ at this angle of incidence, will be linearly polarized perpendicular to the plane of incidence. Thus, the polarization state of the reflected and transmitted light from a plane dielectric surface is not necessarily the same as that of the incident light. Light polarization at θ_B is often employed in laser technology. If the incident light is circularly polarized, the reflected light has reversed handedness of the polarization.

1.4.2 Absorption and scattering

The absorption and scattering by particles in a medium contribute to the extinction of light as it propagates. The amount of light attenuation or extinction along the

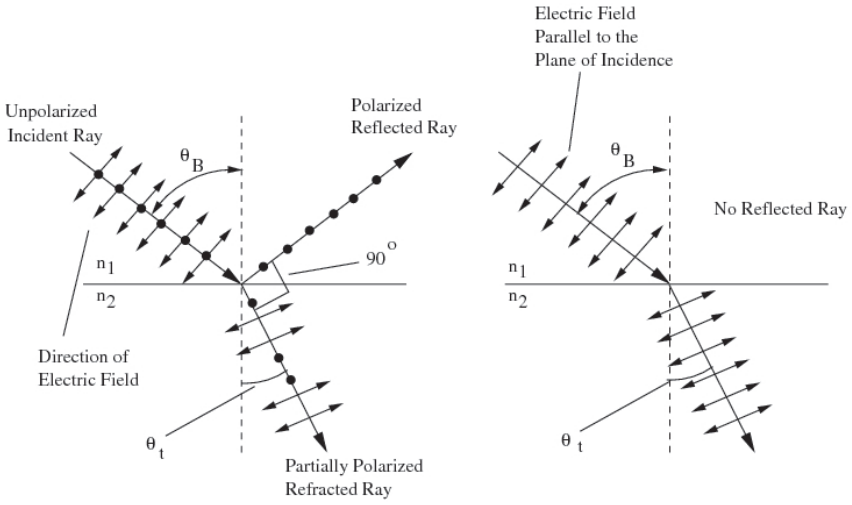

Figure 1.4: Electromagnetic radiation polarized at Brewster angle $\theta_i = \theta_B$, from Ref. [13].

direction of propagation due to absorption and scattering depends on the density, size, and refractive index of the particles. Electromagnetic radiation at a particular frequency ν propagating in the direction $\hat{\Omega}$ in a medium of physical thickness h will be exponentially attenuated due to absorption and scattering according to the following extinction law [14]:

$$I_\nu(z, \hat{\Omega}) = I_\nu(0, \hat{\Omega})\, e^{-\tau(\nu)} \tag{1.15}$$

where $I_\nu(0, \hat{\Omega})$ and $I_\nu(z, \hat{\Omega})$ are the intensities at $z = 0$ and at $z = h$, respectively, and where the optical path length $\tau(\nu)$ is given by

$$\tau = -\int_0^h \mu dz. \tag{1.16}$$

Here the minus sign indicates that τ increases downwards from the upper boundary, μ is the extinction coefficient [m^{-1}], which is equal to the sum of the absorption coefficient μ_a and the scattering coefficient μ_s of the medium, *i.e.* $\mu = \mu_a + \mu_s$. If $\mu_s = 0$, the exponential attenuation is due to absorption only. Absorption increases the internal energy or the temperature of an absorbing medium. It depends on the imaginary part n' of the complex refractive index according to $\mu_a = 4\pi n'/\lambda$, where λ is the wavelength of the absorbed radiation in the medium [10]. Absorbed electromagnetic radiation will be re-emitted according to Stefan-Boltzmann's law [15], and the wavelength of maximum emitted radiation is given by $\lambda_m T = 2897.8\ \mu\mathrm{m\ K}$, where T is temperature of the emitting body. Emissions from the earth, the atmosphere, and the human body are

mostly thermal radiation in the infra-red spectral region. A optically opaque material completely absorbs and stops the transmission of the irradiated light energy.

Light scattering processes are valuable for probing the optical properties of various media. Scattering can be used to characterize the size, shape, and refractive index of scattering particles [16]. Scattering processes can be described in terms of classical physics by treating the light as transverse electromagnetic waves and in terms of quantum physics by visualizing the light as a stream of particles called photons. In quantum theory, light absorption, emission, and scattering are given in discrete packets of energy $h\nu$ per photon, which are associated with the discrete changes in the energy levels of atoms and molecules. The classical scattering theory explains the scattering as radiation emitted from the oscillation of atomic dipoles that are induced by the incident electric field of a light wave. Though the quantum description is superior, the classical description of scattering is still useful due to its pedagogical simplicity [14].

Scattering occurs due to spatial inhomogeneities of the refractive index and also due to multiple reflections at surfaces. Surface scattering is related to the nature of the surface roughness, whereas scattering due to aggregates of particles within a given volume depends on their number density, refractive index, and geometry. The initial direction of light is generally changed after scattering, but often the frequency is not altered. However, if the frequency is changed, light is inelastically scattered. For example, when UVA radiation illuminates our nails, it will generate fluorescent emission of visible light.

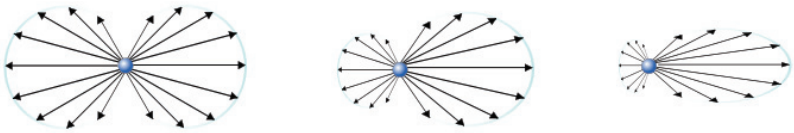

Figure 1.5: Simple illustration of light scattered by different sized spherical particle [20]. Left: Rayleigh scattering, middle and right: Mie scattering. The direction of incident light is from the left to right and the size of particle at the right > the particle in between > the particle at the left.

The effective size of particles is very important in describing the scattering process in a medium. For a sphere of radius r, the effective scattering size or size parameter x is given by the ratio of the circumference of the particle to the wavelength λ in the

medium, *i.e.* $x = 2\pi r/\lambda$. Light scattered by spherical particles can be computed using *Mie* scattering theory [10, 17]. However, there are many non-spherically shaped particles such as aerosols, ice, and several types of biological particles which scatter light differently than spherical particles. The shape of spheroidal particles is characterized by the aspect ratio, and scattering by such non-spherical particles can be described by the T-matrix method [18, 19] as long as the shape does not deviate too much from that of a sphere and the size is not too large.

Small particles

When a particle is sufficiently small, i.e. when $x \ll 1$, the scattering is described by *Rayleigh* scattering theory [17], according to which the intensity I of the scattered light due to unpolarized incident light of intensity I_o is given by

$$I = \left(\frac{\alpha_p}{R}\right)^2 \left(\frac{2\pi}{\lambda}\right)^4 \frac{1+\cos^2\Theta}{2} I_0 \tag{1.17}$$

where R is the distance from the scattering particle to the observation point at a direction specified by the scattering angle Θ, and α_p is the polarizability of the scattering particle and is constant for an isotropic particle. The scattering angle Θ which is function of polar angle ($0 \leq \theta \leq \pi$) and azimuth angle ($0 \leq \phi \leq 2\pi$) is defined in terms of θ and ϕ [see Fig. 1.6] such that

$$\cos\Theta = \cos\theta\cos\theta' + \sin\theta\sin\theta'\cos(\phi' - \phi) \tag{1.18}$$

where $\phi' - \phi$ is the difference between the azimuth angles associated to incident and scattered directions.

Eq. (1.17) shows that the intensity of scattering by particles in the Rayleigh regime is proportional to λ^{-4}. So, blue light of $\lambda = 400$ nm will be scattered five times more than red light of $\lambda = 600$ nm, which is the reason why the clear sky looks blue. Rayleigh scattering is independent of the particle shape [10] as long as the condition $x \ll 1$ is fulfilled. The analytical expression for the Rayleigh scattering cross section is given by [21]

$$Q_{sca}\ (\text{Rayleigh}) = \frac{8\pi}{3}\left(\frac{2\pi}{\lambda}\right)^4 \alpha_p^2 \tag{1.19}$$

where the polarizability α_p of the particle is given by

$$\alpha_p = \frac{m^2-1}{m^2+2} r^3. \tag{1.20}$$

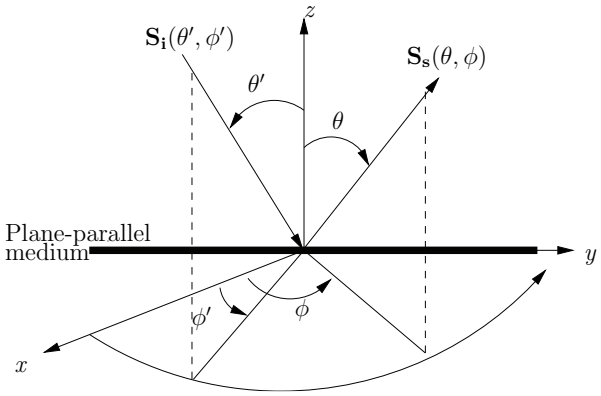

Figure 1.6: Scattering by a volume element located at the center of co-ordinate system. The direction of scattering is specified by $0 \leq \theta \leq \pi/2$ and $0 \leq \phi - \phi' \leq \pi$ measured in the clockwise sense.

Here m is the relative refractive index of particle with respect to the surrounding medium.

Natural light scattered by a Rayleigh scattering medium becomes plane polarized parallel and perpendicular to the scattering plane in the ratio of $\cos^2\Theta : 1$. If the incident light is s polarized, the scattered light is isotropically distributed in all directions. Such scattering is azimuthally independent, implying that Θ becomes independent of ϕ in Eq. (1.18). On the other hand, if the incident light is p polarized, the scattered intensity shows maximum peaks towards the forward and backward directions, but vanishes at $\Theta = \pi/2$. Therefore, the angular distribution of natural light scattered by small particles show a symmetrical scattering pattern around $\Theta = \pi/2$, and the degree of linear polarization P is given by

$$P = \frac{I_\perp - I_\parallel}{I_\perp + I_\parallel} = \frac{1 - \cos^2\Theta}{1 + \cos^2\Theta} \tag{1.21}$$

where the value of P is always positive. For media with anisotropic α_p, the value of P depends on the anisotropy effect [10, 12], and the light scattered at $\Theta = \pi/2$ is not completely polarized. In Rayleigh scattering, the scattering particle or molecule is considered as an individual dipole whose induced dipole moment is proportional to the electric field vector.

Large particle

When $x \simeq 1$, scattering of light by a homogeneous spherical particle is computed

using *Mie* theory [10, 17, 22]. Mie theory computes the scattered light field at a point inside or outside the scattering spherical particle as function of the size parameter x and relative refractive index m. In Mie calculations, the mathematical representation of scattered light including polarization is given by

$$\begin{pmatrix} E_{\parallel s} \\ E_{\perp s} \end{pmatrix} \frac{e^{ik(r-z)}}{-ikr} \begin{pmatrix} S_2(\Theta) & 0 \\ 0 & S_1(\Theta) \end{pmatrix} \begin{pmatrix} E_{\parallel i} \\ E_{\perp i} \end{pmatrix} \tag{1.22}$$

where $0 \leq \Theta \leq \pi$ gives the scattered direction relative to the incident direction in the plane of scattering. $S_1(\Theta)$ and $S_2(\Theta)$ are amplitude functions [17] of the single scattered waves for s and p polarizations and are given by

$$S_1(\Theta) = \sum_{n=1}^{\infty} \frac{2n+1}{n(n+1}[a_n \pi_n(\cos\Theta) + b_n \tau_n(\cos\Theta)] \tag{1.23a}$$

$$S_2(\Theta) = \sum_{n=1}^{\infty} \frac{2n+1}{n(n+1}[a_n \tau_n(\cos\Theta) + b_n \pi_n(\cos\Theta)] \tag{1.23b}$$

where n is summation index. The quantities a_n and b_n are Mie coefficients, which are function of the size parameter and the relative refractive index of the scattering spherical particle, and π_n and τ_n are angular functions related to the associated Legendre polynomials [23], which determine the Θ dependence of the scattered field.

In the forward direction ($\Theta = 0$), S_1 and S_2 become identical. Therefore, the light extinction by an isotropic and homogeneous spherical particle is independent of polarization, and the extinction along the incident direction becomes

$$Q_{ext} = \frac{4}{x^2} \Re\{S(\Theta = 0)\} \tag{1.24}$$

where Q_{ext} is the extinction efficiency factor, *i.e.* the ratio of the extinction cross section to the geometrical cross-section of a sphere and $\Re$ denotes the real part. In terms of the Mie coefficients, the extinction and scattering efficiency factors per particle is given by [17]

$$Q_{ext} = \frac{2}{x^2} \sum_{n=1}^{\infty} (2n+1) Re(a_n + b_n) \tag{1.25a}$$

$$Q_{sca} = \frac{2}{x^2} \sum_{n=1}^{\infty} (2n+1)(|a_n|^2 + |b_n|^2). \tag{1.25b}$$

Eqs. (1.25b) shows that Q_{sca} depends on the size parameter x and the absolute values squared of the Mie coefficients a_n and b_n, suggesting that only the real part of the complex refractive index is involved in scattering. When $x \to 0$, Q_{ext} and Q_{sca} rapidly vanishes, but for $x > 0$, Q_{ext} increases to a maximum value of 4 when $x \approx \lambda$, and deceases to an asymptotic values of 2 when the particle is very large, *i.e.* when $x \gg 1$.

For large particles, the incident light can be represented by a set of geometrical rays. Since the refractive index of the scattering particle differs from that of its surroundings, light will be reflected and refracted according to Snell's law and Fresnel's laws. The amount of the incident light that is extinguished from the propagation direction is proportional to Q_{ext} of the scattering particle. Very large spherical particles show additional Q_{ext} due to diffraction near the surface of the sphere. Therefore, the total extinction by a larg particle becomes twice the value Q_{ext}, which is known as the extinction paradox. Therefore, for very large particles, a sharp intensity peak occurs in the forward direction due to diffraction, and the intensity of this peak is proportional to the geometrical cross section of the scattering particle.

Q_{ext} for a spherical particle is independent of the polarization state of the incident light. However, Q_{ext} depends on the polarization state of the incident light when the scattering particle is non-spherical.

Extinction and scattering efficiencies are dimensionless. But each of the extinction and scattering cross sections of a particle of radius r has the dimension of an area, and are given by $C_{ext} = \pi r^2 Q_{ext}$ and $C_{sca} = \pi r^2 Q_{sca}$, where C_{sca} is the ratio of the scattered light intensity to the incident light intensity per unit of area.

The net extinction is the sum of the extinction due to scattering and that due to absorption. If the extinction does not involve absorption, then $C_{ext} = C_{sca}$. In such a case, the single-scattering albedo is equal to unity. However, the extinction generally involves absorption C_{abs}, and

$$C_{abs} = C_{ext} - C_{sca}. \tag{1.26}$$

Therefore, the value of single-scattering albedo $0 \leq \omega \leq 1$ per particle is given by

$$\omega = \frac{C_{sca}}{C_{abs} + C_{sca}} \tag{1.27}$$

Mie scattering calculations are actually valid for homogeneous spheres of any size. However, the following distinctiions occur when the scattering particles are so small

that Rayleigh scattering occurs.

a) For Rayleigh scattering the forward and backward intensity peaks are symmetric, whereas for Mie scattering, the angular distribution of the scattering is peaked towards the forward direction.

b) For Rayleigh scattering, the polarization is symmetric with respect to Θ. However, for Mie scattering, the maximum polarization is reduced and shifted towards a larger value of Θ as x increases.

c) From Mie scattering calculations, the size of the particles can be determined. However, the size of the particles can not be determined from Rayleigh scattering since the scattering diagram becomes similar for all small particles.

1.4.3 Scattering phase function

The scattering phase function describes the angular distribution of the scattered radiation in terms of the scattering angle Θ, which is angle between the direction of incident radiation and that of the scattered radiation. The single scattering phase function $p(\cos\Theta)$ can be normalized such that

$$\frac{1}{4\pi}\int_{4\pi} d\omega\, p(\cos\Theta) = 1 \tag{1.28}$$

where dω is the differential solid angle centered around the direction of scattering. The phase function is usually expanded as a finite series of Legendres polynomial [14].

$$p(\tau,\mu) \approx \sum_{\ell=0}^{2N-1} (2\ell+1)\chi_\ell(\tau)\, P_\ell \tag{1.29}$$

where τ is the optical depth, $\mu = \cos\Theta$, and $\chi_\ell(\tau)$ is ℓ-th expansion coefficient of the form

$$\chi_\ell(\tau) = \frac{1}{2}\int_{-1}^{1} d\, P_\ell\, p(\tau,\mu), \quad \ell = 0, 1, ...N \tag{1.30}$$

and the ℓ-th polynomial is given by Rodrigues' formula for Legendre polynomial [24]

$$P_\ell = \frac{1}{2^\ell\, \ell!}\frac{d^l}{d\mu^\ell}[(\mu^2-1)^\ell] \tag{1.31}$$

whose first three terms are given by $P_0 = 1, P_1 = \mu,$ and $P_2 = \frac{1}{2}(3\mu^2 - 1)$. The more

asymmetric the scattering phase function, the more expansion terms are required. The zeroth moment χ_0 in (1.30) represents scattering phase function for isotropic scattering. The first moment χ_1 characterizes the shape of the scattering phase function, and is called the *asymmetry factor* g, which is given by

$$g = \chi_1(\tau) = \frac{1}{2}\int_{-1}^{1} d\,\mu\, p(\tau, \mu) \tag{1.32}$$

where g is the average of the cosine of the scattering angle, *i.e.* $g = \langle \cos\Theta \rangle$. g is dimensionless with values lying between -1 and +1. The scattering phase function due to particles with a large size parameter x is peaked towards the forward direction, and the value of g in such cases is within the range of $0 < g \leq 1$. $g = +1$ for complete forward scattering, and $g = -1$ for complete backward scattering. If $g = 0$, the scattering of unpolarized incident light is symmetric around $\Theta = \pi/2$ (Rayleigh scattering). Thus, for Rayleigh scattering, the scattering phase function is given by

$$p(\cos\Theta) \text{ Rayleigh} = \frac{3}{4}(1 + \cos^2\Theta) \tag{1.33}$$

and the asymmetry factor g is zero since the scattering phase function is symmetric around $\Theta = \pi/2$.

Another commonly used scattering phase function in radiative transfer modeling is the Henyey-Greenstein phase function [25]

$$p_{HG}(\cos\Theta, \tau) = \frac{1 - g^2}{(1 + g^2 - 2g\cos\Theta)^{3/2}}. \tag{1.34}$$

This scattering phase function has no physical basis, but may provide a good approximation to a measured scattering phase function. The Henyey-Greenstein (HG) phase function differs from that for Mie scattering particularly in the forward and backward directions, since the HG function does not show any backward peak. The Legendre expansion coefficients for the HG phase function are given by $\chi_\ell(\tau) = g^\ell$.

Observation directions for which $\Theta > \pi/2$ are called forward scattering directions, and observation directions around $\Theta = \pi$ are called backscattering directions. Backscattering is useful in radar and lidar technology for remote sensing of particles.

Collection of particles

An optical medium usually consists of a collection of particles whose size, shape, orientation, and location can be distributed in a random manner. If the collection of particles in a medium are sufficiently far from each other so that the distance between

them is larger than the wavelength of the incident light, then the light scattered by one particle will only to a negligible degree influence the light scattered by other particles. For such an independent scattering process, the scattered intensities due to the different scattering particles can be added. Then the extinction coefficient per unit volume due to a collection of N independently scattering identical particles is given by $N \cdot C_{ext}$, where C_{ext} is the extinction cross section for a single particle.
Optical media consisting of mono-dispersed particles of identical size and shape are rare in the nature. Natural optical media are composed of polydispersed particles, *i.e.* particles of various shapes. For such media, the scattering per particle is given by the ensemble averaged scattering cross-section $\langle C_{ext} \rangle$ where $\langle\ \rangle$ denotes averaging over a size distribution of particles. For a random distribution of particles of various sizes the averaging can be performed using a size distribution function [26, 27], such that

$$\int_{r_{min}}^{r_{max}} n(r)dr = N \tag{1.35}$$

where $n(r)$ [m^{-4}] is the number of particles per unit volume per unit size interval. Thus, $n(r)dr$ gives the number density [m^{-3}] of particles in the size interval between r and $r + dr$, and N [m^{-3}] is the total number of particles per unit volume in the size interval between r_{min} and r_{max}.

The wavelength dependent extinction coefficient $\mu_t(\lambda)$ and the scattering coefficient $\mu_s(\lambda)$ for a size distribution particles are given by

$$\mu_t(\lambda) = \pi \int_{r_{min}}^{r_{max}} r^2\, Q_{ext}(\lambda, r)\, n(r)\, dr \tag{1.36a}$$

$$\mu_s(\lambda) = \pi \int_{r_{min}}^{r_{max}} r^2 Q_{sca}(\lambda, r)\, n(r)\, dr \tag{1.36b}$$

and the corresponding wavelength dependent absorption coefficient is $\mu_a(\lambda) = \mu_t(\lambda) - \mu_s(\lambda)$. Similarly, the ensemble averaged asymmetry factor $\tilde{g}$ is given by

$$\tilde{g}(\lambda) = \frac{1}{\mu_s(\lambda)} \int_{r_{min}}^{r_{max}} C_{sca}(\lambda, r)\, g(\lambda, r)\, n(r)\, dr \tag{1.37}$$

The quantities μ_a, μ_s, and $\tilde{g}$ are specific to a particular optical medium and are called inherent optical properties (IOPs). In radiative transfer problems for plane parallel geometries, the IOPs are generally expressed by the following dimensionless parameters

$$\tilde{\omega} = \frac{\mu_s(\lambda)}{\mu_a(\lambda) + \mu_s(\lambda)} \qquad \tau = -\int_0^z [\mu_a(\lambda) + \mu_s(\lambda)]dz \tag{1.38}$$

where $0 \leq \tilde{\omega} \leq 1$ is size-averaged single-scattering albedo, and τ is the extinction path length along the physical thickness z of the medium. Both τ and z are measured vertically downward from the upper boundary, and $d\tau = -[\mu_a(\lambda) + \mu_s(\lambda)]dz$ contains information about the absorption and scattering properties at different depths in the vertical direction. In an optically homogeneous plane parallel slab, $\tilde{\omega}$ and the scattering phase functions are independent of τ.

Surface scattering

Light scattering from rough surfaces becomes diffuse due to multiple reflections in random directions. Artificial rough surfaces may consist of a spatial distribution of heights and valleys whose dimension ranges from atomic scales to several micrometers [28]. Such a microscopic topography may consist of randomly oriented V-shaped cavities whose oppositely faced planar micro-facets multiply reflect the incident light according to Snell's law into random directions so that the light reflected from the rough surface becomes mostly diffuse [29].

The extent of light diffusion due to rough surface scattering depends on the roughness parameters, which are measured as a height distribution h and a slope distribution α, as shown in Figs. 1.7(a) and 1.7(b), each being a statistically fluctuating variable [30, 31]. Whether a given surface is to be considered smooth or rough, depends also on the wavelength and direction of the incident light. A rough surface will behave as a smooth surface if the wavelength of the incident light is large relative to the roughness parameter [32]. Similarly, the same surface will behave smoother for small grazing angles $(\pi/2 - \theta_i)$ than for large grazing angles. These analytical explanations

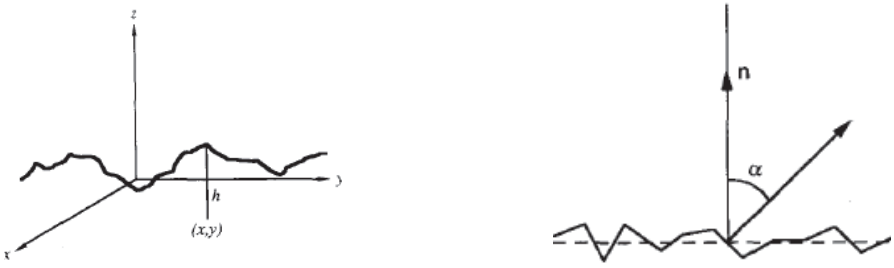

(a) (b)

Figure 1.7: Rough surface as a collection of V-shaped cavities [30]. In (a), the surface height h as a random function of spatial coordinate and, in (b) the surface is modeled as a collection of micro-facets where n is normal to the surface and α is the slope of the facet

of rough surface scattering is valid in both ray optics and wave optics. The ray optics approximation is useful for explaining shadowing and masking when the source and detector are not in the direction of the surface normal. However, the geometrical approximation does not account for interference and diffraction properties of light, which are explained by the wave approach of light propagation. Polarized light is usually depolarized due to surface scattering. However, the degree of depolarization depends on the nature of the surface roughness, the angle of incidence, and the angle of observation.

Light that is multiply scattered either from a surface or due to volume scattering beneath the surface will be randomized and loose its initial direction [see Fig 1.3(b)] so that the direction of the reflected light can be anywhere within a hemisphere ($0 \leq \Theta \leq \pi$). For a given direction and wavelength of the incident light, the reflected light in a specific direction is described by the Bidirectional Reflectance Distribution Function (BRDF) [sr^{-1}], which is the ratio of the reflected radiance [W m^{-2} sr^{-1}] in a specific direction from a given surface area to the incident irradiance [W m^{-2}] upon the same area [33]. The BRDF has the unit of sr^{-1}, can have any value greater than zero, and should be measured by a detector with small field of view.

A homogenous surface that scatters light isotropically in all directions is called a Lambert surface. The reflected radiance from an ideal Lambert surface is independent of the viewing direction. However, such an ideal surface does not exist in nature. Therefore, light scattering from rough surfaces as well as from a volume inside the surface show directional properties, i.e. it is a function of the directions of the incident and scattered light. Spectralon is an artificial diffuse reflectance material that is widely used as a best available light diffuser for practical purposes. We have measured the BRDF for a Spectralon white reflectance standard for incoherent illumination at different directions for wavelengths of 405 and 680 nm of unpolarized and plane polarized light. Our measurements showed deviations of the BRDF for the Spectralon white reflectance standard from that of a Lambertian reflector. These deviations depended both on the angle of incidence and the polarization states of the incident and detected light [34].

1.4.4 Scalar radiative transfer equation

Light can be multiply scattered if the path length between the scattering particles becomes longer than the mean free path between scattering events. In such cases, the light scattered by individual particles will no longer be independent. Simple radiative

transfer of multiple scattering processes in a slab of infinite horizontal extension was formulated by Kubelka and Munk [35, 36] based on the assumption that the distribution of scattered light is vertically upward and downward from the surface. This model does not account for the Fresnel reflection at the surface interface. A change in the refractive index at the interface causes errors in the diffuse limit of scattering [37]. The Monte Carlo method [38] for modeling radiative transfer includes the interface effects. However, this probabilistic approach is found computationally slower [39] compared to the DIscrete Ordinate Radiative Transfer (DISORT) method. DISORT is an efficient and reliable numerical method to model scalar radiation transport in plane-parallel layered medium [40, 41] including the refractive and reflective effects at the surface boundary provided that the IOPs are constant within each of the layers.

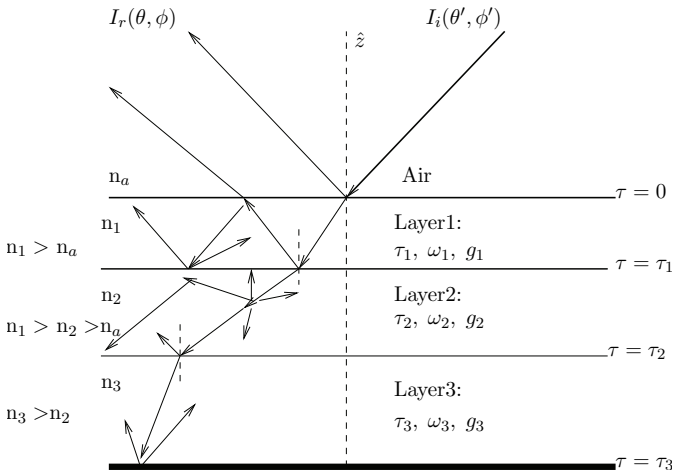

Figure 1.8: Schematic model of a plane parallel optical medium. The inherent optical properties are different in different layers, but they are constant within each layer of given optical thickness τ_i $(i = 0, 1, 2, 3)$ and complex refractive index n_i $(i = a, 1, 2, 3)$.

The scalar equation for transfer of radiation in a plane parallel scattering medium is given by [40, 42]

$$\mu \frac{dI(\tau, \mu, \phi)}{d\tau} = I(\tau, \mu, \phi) - \frac{\tilde{\omega}(\tau)}{4\pi} \int_0^{2\pi} d\phi' \int_{-1}^{+1} du'\, p(\tau, u, \phi; u', \phi') I(\tau, u', \phi') - S^*(\tau, u, \phi) \tag{1.39}$$

where $I(\tau, \mu, \phi)$ is the scalar radiance at a given frequency ν and vertical optical depth τ, $\tilde{\omega}$ is the size-averaged single-scattering albedo, $p(\tau, u, \phi; u', \phi')$ is the scattering phase function describing the scattering from an incident direction $(u' = \cos\theta', \phi')$ to an

observation direction ($u = \cos\theta, \phi$), and the term $S^*(\tau, u, \phi)$ is a source function of scattering given by

$$S^*(\tau, \mu, \phi) = \frac{\tilde{\omega}(\tau)}{4\pi} p(\tau, \mu, \phi; \mu_0, \phi_0) F^0 e^{-\tau/\mu_0} + S_b. \tag{1.40}$$

Here F^0 is the intensity of incident light beam from the direction ($\mu_0 = \cos\theta_0, \phi_0$), and S^b is the diffuse light due to thermal emission into the direction of the incident radiation. For a coupled atmosphere-ocean or air-skin tissue system, the refractive index of air is always less than that of ocean water or skin tissue. If we consider the case of a coupled air-skin system, the single-scattering source term in Eq. (1.40) in the air is

$$\begin{aligned} S^*_{air}(\tau, \mu, \phi) &= \frac{\tilde{\omega}(\tau)}{4\pi} p(\tau, \mu, \phi; -\mu_0, \phi_0) F^0 e^{-\tau/\mu_0} \\ &+ \frac{\tilde{\omega}(\tau)}{4\pi} R(-\mu_0, n_{rel}) F^0 \\ &\times p(\tau, \mu, \phi; \mu_0, \phi_0) e^{-(2\tau_a - \tau)/\mu_0} + S_b \end{aligned} \tag{1.41}$$

Where τ_a is the optical depth of air at the skin surface, $\mu_0 = \cos\theta_0$, where θ_0 the polar angle of the incident radiation, $R(-\mu_0, n_{rel})$ is the reflectance from the interface as given by Eq. (1.14), and n_{rel} is the refractive index of skin relative to that of air. The first term on the right hand side of Eq. (1.42) gives the downward incident beam and the second term describes the upward beam reflected due to the change in the refractive index at the surface boundary. Below the interface, the single-scattering source term becomes [43]

$$\begin{aligned} S^*_{skin}(\tau, \mu, \phi) &= \frac{\tilde{\omega}(\tau)}{4\pi} \frac{\mu_0}{\mu_{0n}} T(-\mu_0, n_{rel}) F^0 \\ &\times p(\tau, \mu, \phi; -\mu_{0n}, \phi_0) \\ &\times e^{-\tau_a/\mu_0} e^{-(\tau - \tau_a)/\mu_{0n}} + S_b \end{aligned} \tag{1.42}$$

where μ_{0n} is the cosine of the angle of transmission θ_{0n} in the skin and $T(-\mu_0, n_{rel})$ is transmittance through the interface.

If we restrict our attention to a plane-parallel slab of thickness τ and consider the azimuthally averaged intensity, Eq. (1.39) simplifies to

$$\mu \frac{dI(\tau, \mu)}{d\tau} = I(\tau, \mu) - \frac{\tilde{\omega}}{2} \int_{-1}^{1} d\omega' p(\tau, \mu', \mu) I(\mu, \tau) - S^*(\tau, \mu) \tag{1.43}$$

where $I(\tau, \mu)$ is azimuthally averaged diffuse radiance or intensity at optical depth τ. For isotropic scattering, the scattering phase function p is equal to unity, and the

single-scattering source function in Eq. (1.40) simplifies to $(\tilde{\omega}/4\pi)\, F^s e^{-\tau/\mu_o} + S_b$.

The radiative transfer equation in (1.39) or (1.43) has no analytical solution; it is solved by numerical methods. One of the common numerical methods is the discrete ordinate method involving Gaussian quadrature, as discussed by Gary and Stamnes [14], Jin et al. [40], and Frette et al. [42], where the integro-differential equation is decomposed into $2N$ coupled differential equations, which are solved using methods of linear algebra.

Research in atmospheric remote sensing has shown that the model based only on scalar radiative transfer are erroneous [5, 44]. Such errors can be significantly reduced if polarization effects are included in the radiative transfer models [45]. Besides, the polarization of the scattered light contains extra information related to the size and shape of scattering particles. Thus, light transport models including polarization effects will be more appropriate for the analysis of light backscattered from thin layered scattering media. However, the measurement of polarized light scattering is not suitable for thick layered multiple scattering media, as the polarization will be completely randomized after few multiple scattering events [46, 47, 48]. The Stokes scattering matrix gives information about the polarization properties of an optical medium. Stokes scattering matrix for light scattering by an elementary skin tissue volume that contains a random distribution of scattering particles is discussed in the third research paper included in this dessertation.

Chapter 2

Light and Human Skin

2.1 Human skin

Skin is the largest organ of the human body with functions in protection, sensation, and thermoregulation. Human skin is composed of three layers: epidermis, dermis, and subcutaneous layers [see Fig. 2.1]. The thickness of each of the three layers varies with body site. Thus, the skin is thicker on the soles and palms and thinner on the eyelids. The epidermis, which is the outermost thin layer, is directly exposed to the outer world.

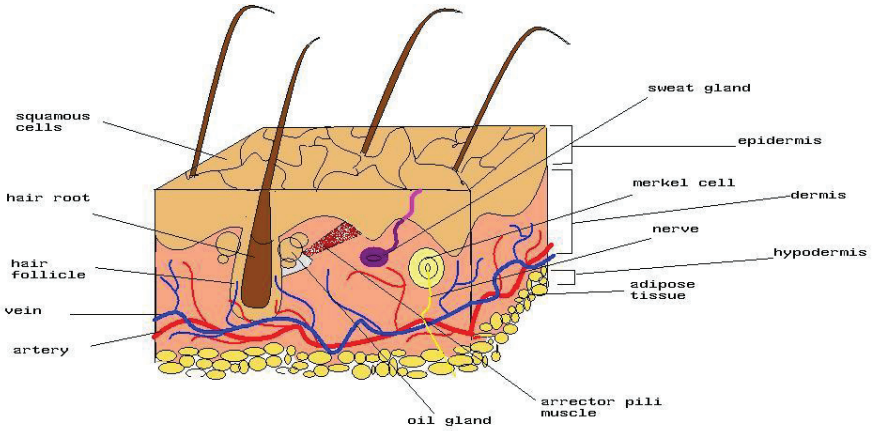

Figure 2.1: Cross-sectional overview of normal human skin with epidermis, dermis, and subcutaneous layers. Picture from Wikimedia commons.

Overexposure of human skin to the short-wavelength part of solar radiation can increase risk of skin cancer, particularly for caucasians. On the other hand, short-time exposure of UVB (λ = 280-315 nm) radiation is beneficial because it synthesizes vitamin D [49,

50], which is essential for the development of the human bone structure as well as for the immune system. In terms of color, human skin is categorized into different types as shown in Table 2.1. The skin color varies with the concentration of melanin pigmentation, which acts as a barrier to the penetration of solar UV radiation into the skin.

Table 2.1: Types of human skin classified according to its relative response to solar exposure [51].

Skin type	Color	Description	Sensibilities to skin cancer
I	White	Never tans, always burns	High
II	White	Sometimes tans, usually burns	High
III	White	Usually tans, may burn	Low
IV	Olive	Always tans, rarely burns	Low
V	Brown	Moderately pigmentated, no burning	Very low
VI	Black	Highly pigmented, no sun burning	Very low

2.1.1 Epidermis layer

The epidermis layer is 0.01-0.1 mm thick and contains melanin pigments and keratin [52, 53] as its main scattering and absorbing particles. This layer has no blood vessels and is fed via the dermis layer, which is below the epidermis. The epidermis is divided into five sub-layers as shown in Fig. 2.2. In the bottom sub-layer, called Stratum basale, new melanosome cells are produced that gradually migrate upwards. The size of the melanosomes decreases as they move upwards from basal layer. Cells in the Stratum spinosum sub-layer are called squamous cells. These cells lose their nuclei and are transported to the stratum corneum sub-layer, which is 10-15 μm thick and composed of dead squamous cells that are glued together with keratin. The melanin concentration varies with the skin type as well as with the body site and gender of individuals [54]. The penetration of solar radiation into the underlying structure of the skin is stongly regulated by the amount of melanin in the epidermis [51,55]. Therefore, the epidermis layer is also called the melanin layer.

2.1.2 Dermis layer

The dermis layer is below the epidermis and is 1 to 3 mm thick. It contains connective tissues, such as blood vessels, sensitive nerves, sebaceous glands, sweat glands, and hair

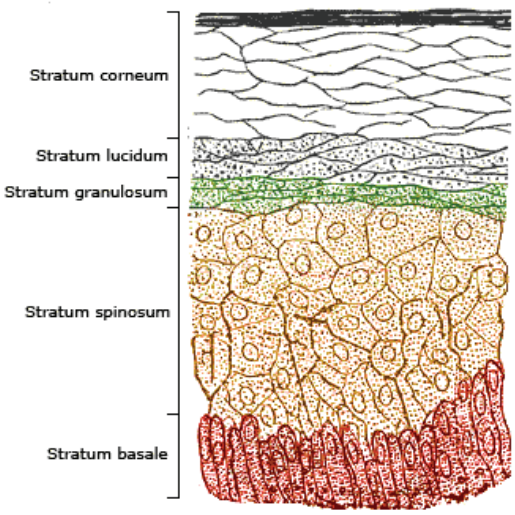

Figure 2.2: Cross-sectional diagram of epidermis with five different sub-layers. From Wikimedia commons.

follicles. The collagen tissues are the most important structural protein tissues in the dermis, making the skin strong and elastic. Collagen, which can represent up to 75% of dermis tissues, show birefringent optical properties [56] due to linear anisotropy of the collagen fibrous structure [57]. The dermis layer regulates the body temperature and transports nutrition by means of blood flow. The nerves give sensations to the brain system of the external environment, such as temperature and injuries. Therefore, the dermis layer is an important layer of the skin. Blood haemoglobin is found in the dermis, and therefore the dermis is also called the hemoglobin layer.

2.1.3 Subcutaneous layer

The subcutaneous layer is below the dermis and is typically 3 mm thick. This layer is also known as the hypo-dermis and is composed mainly of adipose tissues, which consist of connective tissues and fat. The subcutaneous layer acts as insulator and protects the internal organs from external temperature variations. This layer stores energy in the form of fat and is therefore called the fatty layer.

2.2 Optics of human skin tissue

Human skin is a heterogeneous and turbid optical medium in which the propagation of electromagnetic radiation is regulated by its wavelength-dependent absorption and scattering properties. Skin tissues are characterized by stronger scattering than absorption, and the overall absorption properties in the VIS and NIR spectral ranges are determined by the contents of melanin, keratin, blood, and water. These major chromophores show their characteristic photo-biological responses in different spectral bands of interaction with electromagnetic radiation. In the UV spectral band where $\lambda < 400$ nm, the photobiological effects include erythema, photo-carcinogenesis, and melanogenesis [51, 58]. The absorption of light due to melanin and keratin occurs in the epidermis, and this absorption is highest in UV spectral region. Moreover, at short wavelengths, the epidermal transmission is highly influenced by the fluorescence excitation of keratin, an effect that is not very sensitive to radiation at wavelengths greater than 320 nm [52]. The absorption coefficient of melanin in the VIS spectral band decreases with increasing wavelength according to [59]

$$\mu_{a,mel} = 6.17\,\mathrm{mm}^{-1}\left(\frac{\lambda}{1000\,nm}\right)^{-3.48}; \quad \lambda \geq 330\ \mathrm{nm} \tag{2.1}$$

and the absorption of keratin is much higher at wavelengths below 300 nm in the UV spectral region [60].

Oxygenated (HbO_2) and de-oxygenated (Hb) hemoglobin in blood tissues have absorption peaks in the VIS spectral region [61] with maximum absorption at around $\lambda = 405$ nm. Water, which is another major component of tissues, has low absorption in the VIS spectral band but its absorption increases with λ in the NIR spectral band. Thus, the transport of electromagnetic radiation through different depths of skin tissue is highly wavelength dependent. The spectral range having largest penetration within the VIS and NIR spectral bands is known as the *optical window* [62], and is also called the *therapeutic window* [63]. From the spectral position of this window shown in Fig. 2.3, it is clear that red light and NIR radiation propagate deeper into the skin than VIS light at shorter wavelengths. Using light at these red and NIR wavelengths, one may be able to extract information non-invasively about deep tissue layers.

The absorption coefficient $\mu_a(\lambda)$ [m^{-1}] as a function of λ in a medium is given by

$$\mu_a(\lambda) \simeq f_a\,\mu_{a,p}(\lambda) + (1 - f_a)\,\mu_{a,h}(\lambda) \tag{2.2}$$

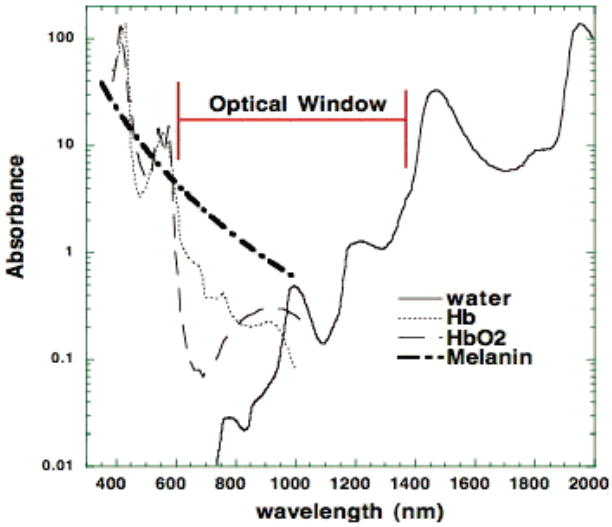

Figure 2.3: Optical window in skin tissue due to reduced absorption of visible and near infrared wavelengths [62].

where f_a is the volume fraction occupied by the absorbing particle, and where $\mu_{a,p}(\lambda)$ and $\mu_{a,h}(\lambda)$ are the absorption coefficients of the particle and the host medium, respectively.

The absorption reduces the intensity of light beam transversing the medium where the absorption coefficient can be experimentally determined by measuring the transmittance T through a tissue slab of thickness z [64]. Thus,

$$\mu_a = \frac{1}{z} \ln \left(\frac{1}{T} \right) \tag{2.3}$$

where μ_a is seen to vary inversely with the physical thickness, implying that it should be small for measurement on samples having large μ_a. The transmittance, which is the ratio of transmitted power $I(z)$ through a thickness z to the incident power $I(0)$ is given by

$$T = \frac{I(z)}{I(0)} = \exp(-\mu_a z). \tag{2.4}$$

When $\mu_a z = 1$, only 37% of light is penetrated through the thickness z, and 63% of the incident light is extinguished due to absorption. The extinction of VIS and NIR radiation in human skin tissue due to absorption is much less than the extinction due

to scattering [52,64]. Before penetration into the tissue volume, a small part of the incident light (≈5%) is reflected from the air-skin interface due to the difference between the refractive indices of air and skin.

Melanosomes and haemoglobin particles in skin tissue both scatter and absorb light. Therefore, the refractive index of these particles is complex. When the host medium is non-absorbing, light absorption is only due to suspended particles. On other hand, when the host medium is absorbing, both the incident and the scattered light will be absorbed depending on the size of the imaginary part of the refractive index. Investigations have shown that an absorbing host medium affects the scattering phase function [65]. Since more than 50% of the volume of biological tissue is filled with water, the host medium or the extra-cellular fluid in skin may have a refractive index that is very close to that of water. The real part of the complex refractive index of the extra-cellular fluid in skin is close to 1.36 in the VIS spectral band [66], and the absorption coefficient of water in the spectral range of λ = 350-700 nm is of the order of 10^{-5} to 10^{-4} [mm^{-1}], which is very small [67].

By considering spherical particles that are embedded in a host medium of real refractive index, one can describe light scattering in skin layers by Mie scattering theory for particles with sizes comparable to the wavelength of the incident light, and Rayleigh scattering theory for particles that are small compared to the wavelength of the incident light. The scattering coefficient $\mu_s(\lambda)$ [m^{-1}] due to contributions from both Mie scattering and Rayleigh scattering can then be expressed by

$$\mu_s(\lambda) \simeq f_s\lambda^{-b} + (1 - f_s)\lambda^{-4} \tag{2.5}$$

where f_s is the fraction of particles contributing to Mie scattering and $(1 - f_s)$ is the fraction of particles contributing to Rayleigh scattering. The exponent b indicates the wavelength dependence of Mie scattering and depends on the size of the particles. Jacques [68] showed that the value of b was the same for particles in the epidermis and the dermis and equal to 0.838. Rayleigh scattering depends on λ^{-4}, and can be expressed as

$$\mu_{s,\mathrm{Ray}}(\lambda) = K\lambda^{-4}, \tag{2.6}$$

where the factor K indicates the magnitude of the Rayleigh scattering component.

Skin tissue consists of randomly positioned particles with shapes that are not well known. The number density and size distribution of particles as well as their refractive indices may vary with position. Thus, the absorption and scattering properties for a

set of polydispersed particles within a unit volume of skin must be averaged according to Eq. (1.35) to provide size averaged optical properties.

Light impinging on the skin surface will be partly transmitted into the underlying skin layers where it will be absorbed and multiply scattered in a random fashion by particles at random positions. Such scattering diffuses the incident light into multiple directions, so that the light backscattered from the skin surface will be anisotropically diffused with anisotropy factor g in the range from 0.7 to 0.95 in the VIS spectral band [64, 68]. As already mentioned, absorption and scattering vary with the size distribution, the refractive index, and the number density of particles. Therefore, the epidermis, dermis, and sub-cutis layers of human skin have different characteristic inherent optical properties. How far a photon will move into the various layers depends on the layer thicknesses dz and the number density of particles in the various layers. The penetration depth of VIS light is not larger than 3 mm [69].

2.2.1 Polarization effects

Natural light, which may be considered to consist of a random mixture of light with different plane polarization states, becomes linearly polarized when it passes through a linear polarizer. An ideal polarizer has complete transmission of one particular polarization state and zero transmission for all other polarization states. Biological tissues are optically anisotropic and show birefringence effects [56,70], which are most likely to occur in the dermis layer mainly due to the presence of non-spherical collagen particles.

Polarized light that propagates in an inhomogeneous skin medium becomes mostly depolarized due to multiple scattering processes. However, if the propagation distance z is such that $z \leq l$ (where $l = 1/\mu_{sca}$ is the transport mean free path for scattering), then single scattering dominates, and single scattering preserves the polarization state of the incident light. On the other hand, if $z \geq l$, multiple scattering occurs, and the polarization state of the incident light will be scrambled. In a scattering medium with spatially uncorrelated Rayleigh scattering particles, the degree of linear and circular polarization due to depolarization of the initial polarization is given by [71]

$$P_i \simeq \frac{2z}{l} \sinh(\frac{l}{\xi_i}) exp(-\frac{z}{\xi_i}) \tag{2.7}$$

where the characteristic depolarization length ζ_i is given by

$$\xi_i = \left(\frac{\zeta_i l}{3}\right)^{1/2}.$$

Here the subscripts $i = L$ and $i = C$ stand for linear and circular polarization, respectively. For $z \gg \zeta_i$, multiple scattering prevails, and then the numerical values for ζ_L and ζ_C can be approximately related by $\zeta_L \simeq 2\zeta_C$ [9]. Thus, the characteristic depolarization length ξ_L for linearly polarized light is 1.4 times longer than the corresponding depolarization length ξ_C for circular polarized light. Eq. (2.7) is also valid for large spherical particles [9, 71] provided the transport mean free path l is replaced by $l^* = 1/\mu'_{sca}$, where $\mu'_{sca} = \mu_{sca}(1-g)$ is the reduced scattering coefficient, which describes the diffusion of light in a random scattering process by including the asymetry factor g.

The radiance of light scattered from skin tissue can be measured for different angular positions of the detector. Light reflected from a skin surface generally consists of a large fraction of diffuse light mixed with a smaller fraction of Fresnel-reflected light. Thus, light backscattered from a skin surface consists of (1) surface glare, which consists of about 5% of the incident light that is Fresnel-reflected, (2) a fraction of light that has been subjected to single scattering from the superficial skin layer and has retained its polarization state, and (3) a large fraction of diffusely backscattered, depolarized light due to multiple scattering in the underlying tissue volume.

The scattered light due to linearly polarized incident light can be measured by setting a polarizer and an analyzer at parallel and perpendicular orientations with respect to the plane of scattering. Parallel orientations of the polarizer and analyzer will transmit both the single-scattering component R_s and the multiple-scattering component R_d, whereas orthogonal orientations of the polarizer and analyzer will transmit only the R_d component by filtering out the R_s component. Thus, by measuring the scattered intensity $I_\parallel$ for parallel orientations of the polarizer and analyzer and the intensity $I_\perp$ for perpendicular orientations of the polarizer and analyzer, we can separate the single-scattering componentR_s from the diffuse-scattering component, such that [72]

$$R_s \propto I_\parallel - I_\perp. \tag{2.8}$$

The degree to which the scattered light retains its initial polarization is given by

$$P = \frac{I_\parallel - I_\perp}{I_\parallel + I_\perp} = \frac{R_s}{R_s + R_d} \tag{2.9}$$

where P is the degree of linear polarization, whose absolute value is bounded by $0 \leq P \leq 1$, with values zero and one corresponding to completely unpolarized ($R_s \to 0$) and completely polarized ($R_d \to 0$) light, respectively. Measurements of polarized light scattering can enable one to discriminate the effect of superficial scattering from the

effect of scattering by deeper tissue structures [73, 74]. Such measurements constitute a non-destructive technique that can be used to investigate skin tumors and micro-circulations in the dermis.

2.2.2 Mueller matrix

The polarization properties of a scattering medium can be represented by a 4×4 matrix, known as the *Mueller matrix*, which charaterizes its optical properties. The elements of the Mueller matrix are mathemathically related to the Stokes vector $\mathbf{S}_\mathrm{i}$ of the incident light and the Stokes vector $\mathbf{S}_\mathrm{s}$ of the scattered light according to

$$\mathbf{S}_\mathrm{s} = \mathbf{M}(\mu)\,\mathbf{S}_\mathrm{i} \tag{2.10}$$

where $\mathbf{M}(\mu)$ is the Mueller matrix of the form [75, 76]

$$\mathbf{M}(\mu) = \begin{pmatrix} m_{11} & m_{12} & m_{13} & m_{14} \\ m_{21} & m_{22} & m_{23} & m_{24} \\ m_{31} & m_{32} & m_{33} & m_{34} \\ m_{41} & m_{42} & m_{43} & m_{44} \end{pmatrix} \tag{2.11}$$

where (μ) is defined by Fig. 1.6 and given in Eq. (1.18). Each elements of $\mathbf{M}(\mu)$ give polarization information related to elastic scattering, which depends on the scattering direction, the refractive index of the medium, the wavelength of the incident light, and the orientation of the scattering volume relative to the polarization direction of the incident light. The elements m_{ij} (where $i,\, j = 1, 2, 3, 4$) are normalized to $|m_{ij}| \leq m_{11} \leq 1$.

Not all 16 elements of Mueller matrix are independent, *i.e.* some elements will be zero or equal to other elements due to symmetry relations. For example, $m_{11} = m_{12} = m_{21} = m_{22} = 1$, and the remaining elements are zero for a horizontal linear polarizer. Similarly, $m_{11} = m_{22} = 1$ and $m_{12} = m_{21} = -1$, and the remaining elements are zero for a vertical linear polarizer. Elements in the third row and third column describes linear polarization along $\pm 45°$. Thus, linear polarization effects can be completely described by 3×3 sub-group elements at the upper left corner of the Mueller matrix.

For a right circular polarizer, $m_{11} = m_{14} = m_{41} = m_{44}$=1, and other elements are zero. Similarly, for a left circular polarizer, $m_{11} = m_{44} = 1$ and $m_{14} = m_{41} = -1$, and the rest of the elements are zero [77]. Thus, circular polarization is described by elements in the fourth row and fourth column of $\mathbf{M}$.

The Mueller matrix of a reflecting isotropic surface or a single-scattering dipole is diagonal [78]. For a perfect depolarizer, which can depolarize the incident polarized light completely, all Mueller matrix elements will be zero, except for the first element m_{11}. But in practice, such a perfect depolarizer does not exist. Biological tissues consist of a collection of particles and have anisotropic scattering properties implying that not all off-diagonal elements of $\mathbf{M}$ are zero. For example, the non-zero off-diagonal elements m_{12} and m_{21} characterize the linear polarization of the scattered light resulting from incident unpolarized light and are always equal when the particles in the scattering medium are spherical. Moreover, when the scattering particles are spherical, $m_{11} = m_{22}$, $m_{33} = m_{44}$, and $m_{34} = -m_{43}$. If $m_{22}/m_{11} \neq 1$, the scattering medium contains aspherical particles. Thus, departure of the ratio m_{22}/m_{11} from unity is a measure of non-sphericity of the scattering particles. The elements m_{44} and m_{33} describe the ellipticity of the scattered light. For spherical particles, they are equal. The element m_{34} is positive at forward and backward scattering angles and is negative at intermediate scattering angles [79] for randomly shaped, large particles. However, for small particles pertaining to Rayleigh scattering, m_{34} and m_{43} tend to zero. In the case of Rayleigh scattering, the Mueller matrix elements m_{ij} depend on the scattering angle but are independent of the size and shape of the particles.

A plane electromagnetic wave that is scattered only once by a single particle is approximately given as a plane wave locally in the far field zone. However, in a multiple scattering medium, particles in an elementary volume can be illuminated both by direct incident light and diffuse light which has already been scattered by other particles. If the scattering by a single particle in a suspension of particles is independent of scattering by other particles in the suspension, the Stokes parameters of the scattered light due to the individual particles can be added, so that the Mueller matrix for the suspension of particles is given by the superposition of the Mueller matrices for the individual particles [80]. Mueller matrix can be determined experimentally by measuring the scattered light transmitted through different orientations of polarizer at far field .

2.2.3 Scattering matrix

The ensemble-averaged Mueller matrix, which is the sum of the matrices of the individual particles in the volume dv, is referred to as the Stokes scattering matrix $\mathbf{F}$. If (i) each randomly oriented particle in the elementary volume has a plane of symmetry, (ii) each unit volume contains the same number of particles and their mirror particles in random orientation, and (iii) particles are small compared to the wavelength of the incident light, then the scattering matrix contains the following eight non-zero

independent elements:

$$\mathbf{F} = \begin{pmatrix} a_1 & b_1 & 0 & 0 \\ b_1 & a_2 & 0 & 0 \\ 0 & 0 & a_3 & b_2 \\ 0 & 0 & -b_2 & a_4 \end{pmatrix}. \tag{2.12}$$

The element $F_{11} \equiv a_1$, which is the scattering phase function, represents the scattering of unpolarized light, and is the only element required when polarization effects are ignored. It satisfies the normalization condition of Eq. (1.28) where $p(\cos\Theta)$ is replaced by a_1. The elements of $\mathbf{F}$, other than a_1, modify the Stokes vector of the incident light into the Stokes vector of the scattered light. Thus, the matrix elements of Eq.(2.12) are required to solve the radiative transfer equation for polarized light in a medium.

Since the shapes of individual scattering particles in skin tissue are not well known, we may assume the scattering particles of skin tissue to be polydispersed spheres imbedded in a non-absorbing host medium of constant refractive index [66]. In Paper II of this thesis, we assumed human skin to be a non-absorbing host medium that contained ensembles of absorbing and scattering spherical particles so that Mie theory could be used to compute the size averaged asymmetry factor of the scattering phase function, as well as the size averaged absorption and scattering coefficients for a specified size distribution of particles having a wavelength-dependent complex refractive index [81]. Using an optimization scheme, we determined a particle size distribution with complex wavelength-dependent refractive-index for each of the four skin layers so as to obtain best possible agreement between the optimized IOPs and those given by an existing bio-optical model [82].

For spherical particles and also for rotationally symmetric particles, $a_1 = a_2$ and $a_3 = a_4$ in Eq. (2.12). Thus, the scattering matrix for a medium consisting of spherical particle has only the following four independent elements:

$$\mathbf{F} = \begin{pmatrix} a_1 & b_1 & 0 & 0 \\ b_1 & a_1 & 0 & 0 \\ 0 & 0 & a_3 & b_2 \\ 0 & 0 & -b_2 & a_3 \end{pmatrix} \tag{2.13}$$

where $a_1,\ a_3,\ b_1$, and b_2 are related to amplitude functions S_1 and S_2 [see Eqs. (1.23a)

and (1.23b)] associated with the electric-field components of the scattered wave.

As already mentioned, the ratio b_1/a_1 gives the degree of linear polarization of incident unpolarized light. At very large scattering angles, the degree of linear polarization due to larger scattering particles becomes negative due to constructive interference of coherently scattered light, whereas the scattering by spheroidal leads to positive degree of linear polarization. Similarly, the ratio a_2/a_1 in the scattering matrix (2.12) provides a measure of the non-sphericity of the scattering particles. Thus, the ratio becomes equal to 1 for spherical particles, but differs from unity for non-spherical particles and shows different values at different scattering angles for differently shaped particles so that prolate and oblate spheroids can be discriminated [19].

The Stokes vectors of the incident and scattered radiation are defined with respect to the plane of scattering, *i.e.* the plane defined by the directions of the incident and the scattered radiation. However, in a multiple-scattering process, the plane of scattering changes from one scattering event to another. Therefore, the meridional plane, *i.e.* the plane containing the direction of the incident (scattered) radiation and the surface normal is used as the reference plane for the Stokes vector of the incident (scattered) radiation. In a multiple-scattering process, each of these meridional planes of reference should be transformed to a fixed laboratory reference frame by rotation [12, 83]. The scattering matrix obtained upon transformation from the local scattering plane to a fixed laboratory frame of reference, is called the phase matrix. The phase matrix is required to solve the radiative transfer equation for polarized light.

2.2.4 Dermatological aspects of polarized light

Skin optics has special relevance to how light can be utilized in skin cancer diagnosis [84] and photodynamic therapy [85]. Light scattered by skin tissue contains morphological information which can be exploited to identify histo-pathological stages of skin deseases, such as cancers and dysplasia[1] without performing a biopsy procedure. Many of the dysplastic[2] nevi are indistinguishable from their sorrounding tissues *in situ* and difficult to detect [86] in their early stages. Malignant melanoma is deadly form of skin cancer which may start to develop from a pigmented nevus. It has been reported that nearly 1000 Norwegians are diagnosed having the Malignant Melonama type of skin cancer every year [87]. Corresponding numbers on a global basis are very large. According to the World Health Organization (WHO) report, one in every three cancers

[1] abnormal alteration in size, shape and growth of adult cells

[2] mole whose appearance is different from that of common moles

diagnosed is skin cancer [88].

Investigations have reported that more than 85% of cancer originate in the epithelial lining and grow downwards [47, 86] and many of them are indistinguishable from their surroundings in their early stages. Melanoma that is only confined to the epidermis layer in-situ has no risk of death, but the survival rates of cancer patients depend on an early diagnosis. The most common procedure for early diagnosis is to carry out a medical biopsy by a trained dermatologist, but biopsy becomes problematic for patients with a larger number of atypical nevi, also called dysplastic nevi. Medical biopsy may become practically impossible [89] when moles are spread over a larger area with 100 or more in number and only few of them turn into melanoma skin cancer [90]. Moreover, the surgical removal of one or few of such moles would not prevent the development of melanoma cancer [91].

Doctors use the ABCD rule for visual identification of malignant melanoma [92], but this rule is not sufficient when a lesion of possible malignant melanoma is at an early stage. Dermatoscopy, which is also known as epiluminescence microscopy, can magnify the feature of the skin lesion and assists dermatologists to visually decide whether the suspected lesion should be surgically removed for laboratory examination. Dermoscopic images obtained from polarized light scattered from the skin can provide characteristic information related to the morphology of skin tissue. Polarized light scattered from the superficial layer is less depolarized than that emerging from the underlying tissues where the polarization becomes greatly deteriorated. Skin images obtained using polarized light can enable one to visualize the true margins of skin cancer which are not visible to dermatologists. Thus, the polarized light scattered from the superficial skin layer can characterize dysplasia carcinomas in situ (CIS), which is an early stage cancer that has not yet invaded into the deeper tissues. Polarized optical coherent tomography (OCT) of skin tissues can reveal birefringence properties [93] and microcirculation in the dermis. Exposure of biological tissues to polarized light has also been used to stimulate biological responses of the immune system [69] to heal some dermatological diseases by BIOPTRON light therapy.
Ther inteaction of light with skin tissue has been intensively investigated to develop non-invasive diagnostic methods [1, 2] for detecting cancer of skin.

The most effective method of protection against the development of melanoma is minimization of ultraviolet exposure from sunlight. Thus, protection from the sun's rays plays a critical role in prevention of malignant melanoma.

Bibliography

[1] D. L. Swanson, S. D. Laman, M. Biryulina, K. P. Nielsen, G. Ryzhikov, J. J. Stamnes, B. Hamre, L. Zhao, F. S. Castellana, and K. Stamnes. Optical transfer diagnosis of pigmented lesions: a pilot study. Skin Res. Technol. **15**, 330–337 (2009). doi: 10.1111/j.1600-0846.2009.00367.x

[2] D. L. Swanson, S. D. Laman, M. Biryulina, K. P. Nielsen, G. Ryzhikov, J. J. Stamnes, B. Hamre, L. Zhao, E. Sommersten, F. S. Castellana, and K. Stamnes. Optical transfer diagnosis of pigmented lesions. Dermatol. Surg. **36**, 1–8 (2010). DOI: 10.1111/j.1524-4725.2010.01808.x

[3] K. P. Nielsen. *A novel approach for imaging objects embedded in tissue*. PhD thesis, University of Bergen. Allegaten 55, 5020 Bergen (2004).

[4] L. Zhao. *A novel approach for imaging objects embedded in tissue (Part II)*. PhD thesis, University of Bergen. Allegaten 55, 5020 Bergen (2004).

[5] D. M. Stam and J. W. Hovenier. Errors in calculated planetory phase functions and albedos due to neglecting polarization. Astron. Astrophys. **444**, 275-286 (2005).

[6] B. H. Bransden and C. J. Joachain. *Physics of Atoms and Molecules*, 2nd edition. Pearson Education Ltd, Essex CM20 2JE, England (2003).

[7] http://en.wikipedia.org/wiki/Electromagnetic_spectrum.

[8] M. Born and E. Wolf. *Principles of Optics*, 7th edition. Cambridge University Press, UK (2006).

[9] C. Brosseau. *Fundamental of Polarized Light – A Statistical Optics Approach*. A Wiley Interscience Publication, USA (1998).

[10] C. F. Bohren and D. R. Huffman. *Absorption and scattering of light by small particles.* A Wiley-VCH, GmbH & Co., Germany (2004).

[11] S. Chandrasekhar. *Radiative Transfer*. Dover Publication, Inc. N.Y. (1960).

[12] J. W. Hovenier, C. Van Der Mee, and H. Dumke. *Transfer of Polarized Light in Planetary Atmospheres*. Astrophysics and space science library, **38**. Kluwer Acamedic Publishers, UK (2004).

[13] *h*ttp://en.wikiversity.org/wiki/File:BrewsterAngle.jpg.

[14] G. E. Thomas and K. Stamnes. *Radiative Transfer in the Atmosphere and Ocean*. Cambridge University Press (2002).

[15] E. Hecht. *0ptics*, 4rth edition. Addison Wesley, USA (2002).

[16] A. R. Jones. Light scattering for particle characterization. Progress in Energy and Combustion Science **25**, 1-53 (1999).

[17] H. C. Van de Hulst. *Light Scattering by Small Particles*. Dover Publications Inc., New York (1957).

[18] P. C. Waterman. Symmetry, unitarity, and geometry in electromagnetic scattering. Phys. Rev. D **3**, 825-839 (1971).

[19] M. I. Mishchenko, L. D. Travis, and D. W. Mackowski. T-matrix computations of light scattering by nonspherical particles: A Review. J. Quant. Spec. Radiat. Transfer **55**, 535-575 (1996).

[20] *h*ttp://fr.wikipedia.org/wiki/Fichier:Mie_scattering.svg.

[21] A. J. Cox, Alan J. Deweerd, and J. Linden. An experiment to measure Mie and Rayleigh total scattering cross sections. Am. J. Phys. **70**, 620-625 (2002).

[22] W. J. Wiscombe. Improved Mie scattering algorithms. Apl. Opt. **19**, 1505-1509 (1980).

[23] W. A. de Rooij and C. C. A. H. Van der Stap. Expansion of Mie scattering matrices in generalized spherical functions. Astron. Astrophys. **131**, 237-248 (1984).

[24] http://en.wikipedia.org/wiki/Rodrigues'_formula.

[25] L. C. Henyey, J. L. Greenstein. Diffuse radiation in the galaxy. J. Astrophys. **93**, 70 - 83 (1941).

[26] M. I. Mishchenko and L. D. Travis. Capabilities and limitations of a current fortran implementation of the T-matrix method for randomly oriented rotationally symmetric scatters. J. Quant. Spectrosc. Radiat. Transfer **60**, 309-324 (1998).

[27] E. Limpert, W. A. Stahel, and M. Abbt. Log-normal distributions across the science: keys and clues. BioScience **51**, 341-351 (2001).

[28] J. M. Bennett, Recent developments in surface roughness characterization. Meas. Sci. Tech. **3**, 1119-1127 (1992).

[29] K. E. Torrance and E. M. Sparrow. Theory for off-specular reflection from roughened surfaces. J. of Opt. Soc. Am. **57**, 1106-1114 (1967).

[30] S. K. Nayar, K. Ikeuchi, and T. Kanade. Reflectance Reflection: Physical and Geometrical Perspectives. IEEE Transaction on pattern analysis and machine intelligence **1**3, (1991).

[31] D. He Xiao, K. E. Torrance, F. X. Sillion, and D. P. Greenberg. A comprehensive physical model for light reflection. Computer Graphics **25**, (1991).

[32] P. Beckmann and A. Spizzichino. *The Scattering of Electromagnetic Waves from Rough Surfaces*, Pergamon Press (1963).

[33] F. E. Nicodemus. Reflectance nomenclature and directional reflectance and emissivity. Appl. Opt. **9**, 1474-1475 (1970).

[34] A. Bhandari, B. Hamre, Ø. Frette, L. Zhao, J. J. Stamnes, and M. Kildemo. Bidirectional reflectance distribution function of Spectralon white reflectance standard illuminated by incoherent unpolarized and plane-polarized light. Appl. Opt. **50**, 2431-2442 (2011).

[35] W. F. Cheong, S. Prahl, and A. J. Welch. A Review of the optical properties of biological tissues. IEEE J. Quant. Electron. **2**6, 2166-2185 (1990).

[36] P. Edström, Examination of the revised Kubelka-Munk theory: considerations of modeling strategies. J. Opt. Soc. Am. A **24**, 548-556 (2007).

[37] B. Chen, K. Stamnes and J. J. Stamnes. Validity of the diffusion approximation in bio-optical imaging. Appl. Opt. **4**0, 6356-6366 (2001).

[38] L. Wang, S. L. Jacques, and L. Zheng. MCML-Monte Carlo modeling of light transport in multilayered tissues. Computer Methods and programs in Biomedicine **47**, 131-146 (1995).

[39] K. I. Gjerstad, J. J. Stamnes, B. Hamre, J. K. Lotsberg, B. Yan, and K. Stamnes. Monte Carlo and discrete-ordinate simulations of irradiances in the coupled atmosphere-ocean system. Appl. Opt. **4**2, 2609-2622 (2003).

[40] Z. Jin and K. Stamnes. Radiative transfer in nonuniformly refracting layered media: atmosphere-ocean system. Appl. Opt. **33**, 431-442 (1994).

[41] Yan, B. Yan and K. Stamnes. Discrete ordinate radiative transfer coupled atmosphere-ocean system. Analytic complete radiance distributions. J. Quant.Spec. Radiat. Trans. **76** 207-223 (2003).

[42] Ø. Frette, J. J. Stamnes and K. Stamnes. Optical remote sensing of marine constituents in coastal waters: a feasibility study. Appl. Opt. **37**, 8318-8326 (1998).

[43] K. Hestenes, K. P. Nielsen, L. Zhao, J. J. Stamnes and K. Stamnes. Monte carlo and discrete-ordinate simulations of spectral radiances in a coupled air-tissue system. Appl. Opt. **46**, 2333-2350 (2007).

[44] O. V. Postylyakov. Linearized vector radiative transfer model MCC++ for a spherical atmosphere. J. Quant. Spec. Radiat. Transfer **88** 297- 317 (2004).

[45] F. M. Schulz, K. Stamnes, and F. Weng. VDISORT: An improved generalized discrete ordinate method for polarized (vector) radiative transfer. J. Quant. Spectrosc. Radiat. Transfer **61**, 105-122 (1999).

[46] A. Vitkin and R. C. N. Studinski. Polarization preservation in diffusive scattering from in vivo turbid biological media: effects of tissue optical absorption in the exact backscattering direction. Opt. Commun. **190**, 37-43 (221).

[47] Y. L. Kim, Y. Liu, R. K. Wali, H. K. Roy, M. J. Goldberg, A. K. Kromin, K. Chen, and V. Backman. Simultaneous measurement of angular and spectral properties of light scattering for characterization of tissue microarchitecture and its alteration in early precanccer IEEE J. Quant. Electro. **9**, 243-256 (2003); DOI: 10.1109/JSTQE.2003.814183.

[48] Y. Liu, Y. l. Kim and V. Backman. Development of a bioengineered tissue model and its application in the investigation of the depth selctivity of polarized gating. Appl.Opt. **44**, 2288-2299 (2005).

[49] N. G. Jablonski and G. Chaplin. The evolution of human skin coloration. J. Human Evolution **3**9, 57-106 (2000). doi:10.1006/jhev.2000.0403.

[50] K. P. Nielsen, L. Zhao, J. J. Stamnes, K. Stamnes, and J. Moan. Importance of the depth distribution of melanin in skin for DNA protection and other photobiological processes. J. Photochem. Photobiol. **82**, 194-198 (2006).

[51] A. R. Young. Chromophores in Human Skin. Phys. Med. Biol. **42**, 789-802 (1997).

[52] R. R. Anderson, B. S. and J. A. Parrish. The optics of human skin. J. Invest. Dermat. **77**, 13-19 (1981).

[53] S. Alaluf, D. Atkins, K. Barrett, M. Blount, N. Carter, and A. Heath. Ethnic variation in melanin content and composition in photoexposed and photoprotected human skin. Pigment Cell Research **15**, 112118 (2002). doi: 10.1034/j.1600-0749.2002.1o071.x

[54] J. Sandby-Møller,T. Paulsen, and C. Wulf. Epidermal thickness at different body sites: relationship to age, gender, pigmentation, blood content, skin type, and smoking. Acta Derm. Venereol. **83**, 410-413 (2003).

[55] M. A. Pathak. Sunscreens: Topical and systemic approaches for protection of human skin against harmful effects of solar radiation. J. Am. Acad. Derma. **7**, 285-312 (1982).

[56] S. R. Sharma, R. Poddar, P. Sen, and J. T. Andrews. Effect of vitamin C on collagen biosynthesis and degree of birefringence in polarization sensitive optical coherence tomography (PS-OCT). Afric. J. Biotech. **7**, 2049 - 2054 (2008).

[57] X. Wang and L.V. Wang. Propagation of polarized light in birefringent turbid media: A Monte Carlo study. J. Biomed. Opt. **7**, 279-290 (2002).

[58] B. L. Diffey. A Mathematical model for ultraviolet optics in skin. Phys. Med. Biol. **28**, 647-657 (1983).

[59] S. L. Jacques and D. J. McAuliffe. The melanosome: Threshold temperature for explosive vaporization and internal absorption coefficient during pulsed laser irradiation. Photochem. Photobiol. **53**, 69-75 (1991).

[60] E. G. Bendit and D. Ross. A Technique for Obtaining the Ultraviolet Absorption Spectrum of Solid Keratin, Appl. Spectrosc. **15**, 103-105 (1961).

[61] D. J. Faber, M. C. G. Aalders, E. G. Mik, B. A. Hooper, M. J. C. van Gemert, and T. G. van Leeuwen. Oxygen saturation-dependent absorption and scattering of blood. Phys. Rev. Lett. **93**, 1-4 (2004).

[62] *h*ttp://www.photobiology.info/Hamblin.html.

[63] J. Mobley and T. V. Dinh, Optical properties of tissue. *Biomedical Photonics Handbook*, Chapter 2, CRC Press (2003).

[64] M. J. C. Van Gemert, S. L. Jacques, H. J. C. M. Sterenborg, and W. M. Star. Skin Optics. IEEE Trans. Biomed. Eng. **36**, 1146-1154 (1989).

[65] Q. Fu and W. Sung. Mie theory for light scattering by a spherical particle in an absorbing medium. Appl. Opt. **40**, 1354-1361 (2001).

[66] R. Drezek, A. Dunn, and R. Richards-Kortum. Light scattering from cells: finite-difference, time-domain simulations and goniometric measurements. Appl. Opt. **38**, 3651-3661 (1999).

[67] D. J. Segelstein. The complex refractive index of water. M.Sc. thesis, University of Missouri, Kansas City, 1981.

[68] S. L. Jacques. Optical assessment of cutaneous blood volume depends on the vessel size distribution: a computer simulation study. J. Biophoton. **3**, 75-81 (2010). DOI 10.1002/jbio.200900085.

[69] J. Begic-Rahic and S. Vranic. The application of bioptron light therapy in dermatology and wound healing. European Dermatology **5**. 57-60 (2010).

[70] M. Pircher, E. Goetzinger, R. leitgeb, and C. K. Hitzenberger. Three dimensional polarization sensitive OCT of human skin in vivo. Opt. Exp. **12**, 3236-3244 (2004).

[71] V. V. Tuchin. *Tissue Optics. Light Scattering Methods and Instruments for Medical Diagnosis*, 2nd edition. SPIE publication, Washington, USA (1998).

[72] S. L. Jacques, J. C. Ramella-Roman, and K. Lee. Imaging skin pathology with polarized light. J. Biomed. Opt. **7**, 329-340 (2002).

[73] J. O. Doherty, J. Henricson, C. Anderson, M. J. Leahy, G. E. Nilsen, and F. Sjøberg. Sub-epidermal imaging using polarized light spectroscopy for assessment of skin microcirculation. Skin Res. Tech. **13**, 472-484 (2007).

[74] Y. Pan, D. S. Gareau, A. Scope, M. Rajadhyaksha, N. A. Mullani, and A. A. Marghoob. Polarized and nonpolarized dermoscopy- the explanation for the observed differences. Arch. Dermatol. **144**, 828-829 (2008).

[75] A. B.-David. Mueller matrices and information derived from linear polarization lidar measurements: theory. Appl. Opt. **37**, 2448-2463 (1998).

[76] A. H. Hielscher, A. A. Eick, J. R. Mourant, D. Shen, J. P. Freyer, and I. J. Bigio. Diffuse backscattering Mueller matrices of highly scattering media. Opt. Express **1**, 441-453 (1997).

[77] R. A. Chipman. *Handbook of Optics*, **1** 3rd. edition, Chap.14. McGraw-Hill, USA (2010).

[78] J. Ellis, P. Caillard, and A. Dogariu. Off-diagonal Mueller matrix elements in backscattering from highly diffusive madia. J. Opt. Soc. Am. A **19**,43-48 (2002).

[79] M. I. Mishchenko and L. D. Travis. Light scattering by polydispersions of randomly oriented spheroids with sizes comparable to wavelengths of observation. Appl. Opt. **30**, 7206-7223 (1994).

[80] K. J. Voss. Measurement of Mueller matrix for ocean water. Appl. Opt. **23**, 4427-4439 (1984).

[81] A. Bhandari, B. Hamre, Ø. Frette, K. Stamnes, and J. J. Stamnes. Modeling optical properties of human skin using Mie theory for particles with different size distributions and refractive indices. Opt. Express **19**, 14549-14567 (2011).

[82] *h*ttp://www.baltermedical.com/.

[83] S. Bartel and A. H. Hielscher. Monte Carlo simulations of the diffuse backscattering Mueller matrix for highly scattering media. Appl. Opt. **39**, 1580-1588 (2000).

[84] R. J. Friedman, D. S. Rigel, and A. W. Kopf. Early detection of Malignant melanoma: the role of physician examination and self-examination of skin. CA Cancer J. Clin. **35**, 130-151 (1985).

[85] E. J. Dennis, G. J. Dolmans, R. K. Jain, and D. Fukumura. Photodynamic therapy for cancer. Nature Reviews Cancer **3**, 380-387 (2003).

[86] L. T. Perelman and V. Backman. Light scattering spectroscopy of epithelial tissue: principle and apllications. *Handbook of Optical Biomedical Diagnosis*, chapter 12. 675-720 (2002).

[87] *h*ttp://www.kreftregisteret.no/.

[88] *h*ttp://www.who.int/uv/faq/skincancer/.

[89] D. S. Rigel and J. A. Caruncci. Malignant Melanoma: prevention, early detection, and treatment in the 21st century. CA cancer J. Clin. **50** 215-236 (2000).

[90] R. J. Friedman, M. J. Farber, and M. A. Warycha. The dysplastic. nevus. Clin. Dermatol. **27**, 103115 (2009).

[91] A. G. Goodson and D. Grossman. Strategies for early melanoma detection: approaches to the patient with nevi. J. Am. Acad. Dermatol. **60**, 719738 (2009).

[92] W. Stolz, A. Rieman, A. B. Cognetta, L. Pillet, W. Abmayr, and D. Holzel. ABCD rule of dermatoscopy: a new practical method for early recognition of malignant melanoma. Eur. J. Dermatol. **4**, 521-527 (1994).

[93] M. C. Pierce, J. Strasswimmer, B. H. Park, B. Cense, and J. F. de Boer. Birefringence measurements in human skin using polarization-sensitive optical coherence tomography. J. Biomed. Opt. **9**, 287 (2004); doi:10.1117/1.1645797.

[94] J. Kim, R. John, P. J. Wu, M. C. Martini, and J. T. Walsh Jr. In vivo characterization of human pigmented lesions by degree of linear polarization image maps using incident linearly polarized light. Lasers in Surgery and Medicine **42**, 76-85 (2010).

[95] E. Collett. Mueller-Stokes matrix formulation of Fresnel's equation. Am. J. Phys. **39**, 517-528 (1971).

[96] http://commons.wikimedia.org/wiki/Human_skin.

Chapter 3

Overview of reseach papers and conclusions

In the previous chapters, the general bevavior of visible and near-infrared electromagnetic radiation in human skin tissues, including absorption, scattering, and polarization is discussed. The knowledge of how light interacts with human skin tissue and is transported through different tissue layers is important for the development of non-invasive optical methods that can be used to evaluate the physiological state of normal and abnormal skin tissues. This thesis includes four research papers that are dealing with the optical nature of highly scattering media, such as Spectralon reflecting standards and normal skin tissue.

3.1 Research papers

Paper I

Bidirectional reflectance distribution function of Spectralon white reflectance standard illuminated by incoherent unpolarized and plane-polarized light.
Published in Applied Optics **50**, 2431-2442 (2011).

In this paper, we discuss measurements and descriptions of the Bidirectional Reflectance Distribution Function (BRDF) of a Spectralon white reflectance standard, which is CIE (International Commission on Illumination) recommended light diffusing standard that is widely used as a reference standard for the calibration of photometric instruments on the ground as well as on-board satellites. In the visible spectral range, the hemispherical reflectance of this reflectance standard is claimed to be larger than

98% with Lambertian characteristics. In this paper it is discussed how the angular distribution of the scattered light varies when light of two different wavelengths is incident from different directions, and is either plane polarized or unpolarized. This knowledge constitues a fundamental step towards the understanding of how incoherent unpolarized or plane polarized light is scattered by a Spectralon white reflectance standard, which is assumed to an isotropically scattering surface.

I performed the measurements and analyzed the data, and I wrote the manuscript of this paper together with the co-authors. The starting ideas came from my supervisor Jakob Stamnes.

Paper II

Modeling optical properties of human skin using Mie theory for particles with different size distributions and refractive indices.
Published in Optics Express **19**, 14549-14567 (2011).

In this paper, we used size distributions of spherical particles with complex, wavelength-dependent refractive index to compute the inherent optical properties (IOPs) in four different layers of human skin at ten different wavelengths in the visible and near-infrared spectral bands. Since the sizes and shapes of particles in skin tissues are not well known, we considered the particles to be randomly distributed spheres of different sizes, so that we could apply Mie theory to compute the IOPs. Further, we used an optimization scheme to compare the IOPs obtained from Mie computations with those obtained from a bio-optical model. The optimized, size-averaged absorption coefficient, scattering coefficient, and asymmetry factor for the collection of particles in a host medium can be used to compute the Stokes scattering matrix, which is a required input to model polarized light transport in human skin tissue.

The main ideas came from Jakob Stamnes and Knut Stamnes. I calculated the IOPs using Mie theory and optimized them through comparisons with the IOPs obtained from a bio-optical model. Børge Hamre made a major contribution to the bio-optical model. I wrote the manuscript in collaboration with all co-authors.

Paper III

The Stokes scattering matrix for human skin.

To be submitted for publication.

In this paper, we used a layered model of human skin, as explained in Paper II, to compute the Stokes scattering matrix at five different wavelengths in the visible spectral band. The Stokes scattering matrix explains how the polarization state of light that is incident upon a scattering medium and given in terms of an incident Stokes vector, is transformed to provide the polarization state of the scattered light, given by the scattered Stokes vector, for scattering by particles in a turbid medium, such as a biological tissue.

The ideas follow as a continuation of those in Paper II. I calculated the particle size distribution and their wavelength-dependent complex refractive indices in each layer according to the method explained in Paper II and used the optimized particles size distributions and refractive indices in a FORTRAN code to find the elements of the scattering matrix. Snorre Stamnes made a major contribution to revise and implement the FORTRAN code.

The Stokes scattering matrices presented in this paper are to be used in a polarized radiative transfer code for the coupled air-tissue system to compute the polarized reflectance, and examine how it depends on the vertical structure of skin inherent optical properties including the phase matrix. Since the radiative transfer model that we plan to use for polarized radiative transfer in a coupled air-skin system is not yet fully tested, the work mentioned above will be performed in the near future, after which this paper will be submitted for publication.

Paper IV

Spectral radiance imaging of human skin tissue: theoretical aspects and empirical results.
Presented at Optical Imaging 2006 - Fifth Inter- Institute Workshop on Optical Diagnostic Imaging from Bench to Beside at the National Institutes of Health. Organized by SPIE (2006). Abstract at p. 101 of workshop program.

In this paper, we presented measured spectral radiances reflected from skin that included a pigmented nevus, which was illuminated from different directions. The image analysis included calibration and the application of the discrete ordinate solution of the radiative transfer equation for modeling measured results.

I contributed to scan several pigmented skin lesions at the Haukeland University Hospital in order verify the reprodicibility of a prototype skin camera that was designed and developed by the optics group of the Department of Physics and Technology, University of Bergen. Moreover, my contribution included the calibration of scanned images with reference to the Spectralon white reflectance standard discussed in Paper I.

3.2 Conlusions

This research project is related to an extensive research activity initiated by my supervisor Jakob Stamnes with the goal to design and develop a medical device that can be used by doctors to diagnose skin cancer. The diagnostic procedure is theoretically based on transport of light in a coupled air-skin system and the use of an instrument that scans images of skin containing one or more suspicious lesions. These images needs to be calibrated against a known reflectance standard. Spectralon white standards, which are thought to be perfect, industrially produced light scattering objects are used to calibrate raw images of skin lesions. We examined the scattering nature of such a Spectralon white standard using polarized and unpolarized incident light and found that the scattering by Spectralon varied strongly with the angle of incidence, the angle of scattering, and the polarization state of the incident light. Our conclusion from this work is that the Spectralon will show isotropic scattering only when the direction of incidence is close to being parallel with the normal to the scattering surface.

Skin tissue is an inhomogeneous optical medium due to the variation of the refractive index for various constituent particles. Skin tissue is composed of random particles of different types, each type having specific inherent optical properties (IOPs) determined by their sizes, shapes, and refractive indices. We considered skin particles to be spheres of different sizes and wavelength-dependent refractive indices, and used a lognormal size distribution to determine the IOPs of each skin layer. The IOPs, i.e. the absorption and scattering coefficients and the scattering phase function of skin at different wavelengths, are of interest to skin biologists and dermatologists as well as to the cosmetic skin industry.

With polarization measurements it is possible to separate the surface glare and in-depth diffuse reflection from the subsurface singly-scattered reflected light, which reveals information with a better contrast of the subsurface topography, where skin tissue disorders usually originate. The computed size distributions and wavelength-dependent

refractive indices presented in this thesis can be used to model polarized radiation transport in skin tissues by considering it to be composed of several homogeneous layers, each having its own specific IOPs.